TECHNICAL REPORT ARBRL-TR-02513

RESULTS OF FEASIBILITY STUDY ON COMPUTER ASSISTED TOMOGRAPHY FOR BALLISTIC APPLICATIONS

Csaba K. Zoltani
Kevin J. White
Richard P. Kruger

August 1983

US ARMY ARMAMENT RESEARCH AND DEVELOPMENT COMMAND
BALLISTIC RESEARCH LABORATORY
ABERDEEN PROVING GROUND, MARYLAND

Destroy this report when it is no longer needed.
Do not return it to the originator.

Additional copies of this report may be obtained from the National Technical Information Service, U. S. Department of Commerce, Springfield, Virginia 22161.

The findings in this report are not to be construed as an official Department of the Army position, unless so designated by other authorized documents.

The use of trade names or manufacturers' names in this report does not constitute indorsement of any commercial product.

UNCLASSIFIED

SECURITY CLASSIFICATION OF THIS PAGE (When Data Entered)

REPORT DOCUMENTATION PAGE

READ INSTRUCTIONS BEFORE COMPLETING FORM

1. REPORT NUMBER: TECHNICAL REPORT ARBRL-TR-02513	2. GOVT ACCESSION NO.: AD-A133 214
3. RECIPIENT'S CATALOG NUMBER	
4. TITLE (and Subtitle): RESULTS OF FEASIBILITY STUDY ON COMPUTER ASSISTED TOMOGRAPHY FOR BALLISTIC APPLICATIONS	5. TYPE OF REPORT & PERIOD COVERED: Technical Report
	6. PERFORMING ORG. REPORT NUMBER
7. AUTHOR(s): Csaba K. Zoltani, Kevin J. White, Richard P. Kruger*	8. CONTRACT OR GRANT NUMBER(s)
9. PERFORMING ORGANIZATION NAME AND ADDRESS: US Army Ballistic Research Laboratory, ATTN: DRDAR-BLI, Aberdeen Proving Ground, Maryland 21005	10. PROGRAM ELEMENT, PROJECT, TASK AREA & WORK UNIT NUMBERS: 1L161101A91A
11. CONTROLLING OFFICE NAME AND ADDRESS: US Army Armament Research & Development Command, US Army Ballistic Research Laboratory (DRDAR-BLA-S), Aberdeen Proving Ground, MD 21005	12. REPORT DATE: August 1983
	13. NUMBER OF PAGES: 56
14. MONITORING AGENCY NAME & ADDRESS (if different from Controlling Office)	15. SECURITY CLASS. (of this report): UNCLASSIFIED
	15a. DECLASSIFICATION/DOWNGRADING SCHEDULE

16. DISTRIBUTION STATEMENT (of this Report)

Approved for public release; distribution unlimited.

17. DISTRIBUTION STATEMENT (of the abstract entered in Block 20, if different from Report)

18. SUPPLEMENTARY NOTES

*Los Alamos National Laboratory
WX-3, Fabrication and Assembly, MS C914
Los Alamos, NM 87545

19. KEY WORDS (Continue on reverse side if necessary and identify by block number)

Tomography
X-ray
Reconstruction Algorithm
Ballistic Diagnostics
Computed Tomography

20. ABSTRACT (Continue on reverse side if necessary and identify by block number)

(dll)

Tomography, a noninvasive technique relying on the use of x-ray absorption characteristics of a body taken at multiple angles, allows, through the use of mathematical reconstruction techniques, the determination of unknown density distributions within an object. Here we describe the requirements on such a system for ballistic applications, especially for the study of two-phase flow in a chamber under actual firing conditions. The results of experiments on a static mock-up were used to (Continued on Back)

DD FORM 1 JAN 73 1473 EDITION OF 1 NOV 65 IS OBSOLETE

UNCLASSIFIED

SECURITY CLASSIFICATION OF THIS PAGE (When Data Entered)

20. ABSTRACT (CONTINUED):

illustrate the possibilities and limitations of the proposed system. The mock-up consisted of a fiberglass chamber loaded with inert granular propellant. 180 sets of projection data were taken by moving in a semicircle around the object and stepping by one degree each time. Two different algorithms were used to reconstruct the cross-sectional image of the chamber and propellant grain distribution. Transient ballistic requirements dictate that as few as possible views, i.e., x-ray sources, be used in the actual system design. With 180 views, excellent reconstruction images were obtained. Details such as propellant perforations (1.0 mm) are easily observed. Even with 15 to 20 views, reasonable reconstruction can be achieved and will be the basis of the initial BRL design. The quality deteriorated when only nine (9) views were used in the reconstruction.

One-dimensional Monte Carlo radiation transport calculations were performed for a chamber of various wall thicknesses and materials containing propellant. This configuration simulated a gun chamber. The calculations gave the scattered, transmitted and absorbed photon fraction and energy distribution as a function of x-ray energy input. For a typical chamber configuration, from 3% to 24% of the x-ray energy is transmitted to the detector. The ratio of forward scattered photon fraction to transmitted photon fraction was found to decrease with increasing input x-ray energy although the code could not give an angular distribution. Image contrast calculations were also carried out by varying the amount of propellant in the chamber and determining the variation of the transmitted and scattered photon fraction. Results indicated no contrast problem in this area. Finally, a description of the source, the detectors, the problems attendant upon the x-ray spectrum variation, an overview of the image reconstruction techniques, and the layout of the system to be built at the Ballistic Research Laboratory (BRL) are given.

TABLE OF CONTENTS

LIST OF FIGURES

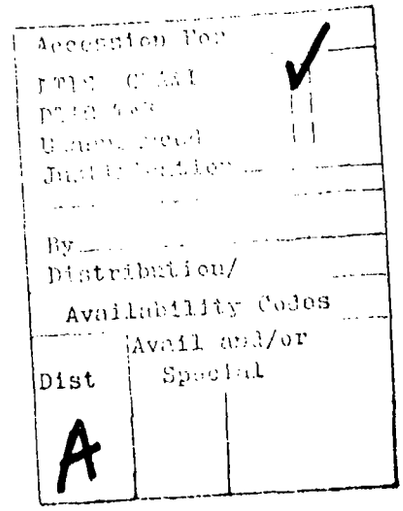

LIST OF TABLES

1. INTRODUCTION

This study was undertaken to demonstrate the feasibility of using tomography to obtain ballistic data which was heretofore either inaccessible or very difficult to obtain. It is based on the premise that an interdisciplinary approach, using insights gained within the last decade in medical radiology as well as computational algorithms, though unfamiliar to most ballisticians, could help in the development of a new experimental technique with a considerable payoff potential. This first report, in the ballistic context, details our initial findings and is subdivided into the following sections. First, the general theory of tomography is outlined with an overview of the reconstruction algorithm. Next, the ballistic requirements are discussed including the insights gained from radiation transport calculations to determine the energy requirements needed for the x-ray sources as well as an estimate on the amount of scattered radiation. In the following section, the results of static experiments are described which established the lower limit on the number of views required for an adequate reconstruction. The proposed BRL system is introduced in Section 5 with the advantages and disadvantages of the various arrangements, and choices of sources and energies are detailed. Section 6 presents information on available detection systems. The report concludes with an overall assessment of the accomplishments and gives the areas where additional work is planned.

2. PRINCIPLES OF TOMOGRAPHY

2.1 What is Tomography?

Tomography is a noninvasive radiographic technique which allows the reconstruction of cross sections of density distributions inside an object from a finite set of its measured x-ray projection values. Its implementation requires a large number of x-ray projection data taken at several view angles around the object and an efficient algorithm implemented on a computer with a large data storage capability. The whole process is usually referred to as computed tomography (CT). The access to cross-sectional density distributions offers the ballistician a unique tool for the study of phenomena heretofore inaccessible to experimentation or, indeed, observation. While conventional methods can give either a local value or an integrated value of a parameter, such as density, by means of tomography, the actual distribution of the parameter through a cross section of the region of interest may be obtained. In addition, the method is noninvasive. Therein lies the tremendous advantage that this new technique confers. Multiphase flow phenomena inside the gun tube, closed bomb experiments, liquid propellant dynamics inside the chamber, actual fragment dispersion while in flight, and dynamic mechanical loading of materials are but a few of the many possible applications of computed tomography.

It is only within the last decade that the full potential of tomography was realized and put to use in medicine for the detection of density differences, i.e., tumors in the human body. It is a giant step beyond the conventional x-ray whose limitations are readily apparent. One only has to recall that a radiograph is a projection of the x-ray absorption of a body onto a two-dimensional planar detector, usually an x-ray sensitive film. Such

a system offers excellent spatial resolution - ten line pairs per millimetre is quite feasible - but the contrast resolution is rather poor. Several limiting factors are important here: First, the shadowgraph is a superposition of the attenuation of the x-ray by the materials between the source and the detector; thus, there may be unwanted shadows of objects which are of no interest. Second, scattering of the x-ray during its traverse of the object can produce fogging. Third, the dynamic range of the film may not be adequate for the resolution of necessary details. Computed tomography overcomes many of these limitations and gives, for the first time, an accurate "inside view" of the object without overlapping shadows or artifacts.

A typical CT layout, see Figure 1, consists of an x-ray source, an object to be studied, and an x-ray detector, usually a scintillation counter. Each detector element produces a signal indicating the attenuation along the ray path between the detector and the x-ray source. Any detector system, including photographic film can, in principle, be used to record the data for the projections. These data are then digitized and subsequently used in the reconstruction of the cross-sectional image. The x-ray beam is collimated into a thin (1.5 - 10 mm) fan that lies at an angle to the major axis of the object being studied. The experiment proceeds by making measurements of the transmitted x-ray signal as the source is moved in a semicircle around the object. Typically, an exposure is taken at one-degree intervals. This will yield 180 different projections. The source is far enough from the detector array so that the object is completely enveloped by the fan of the x-ray beam. Figure 2 shows details of the source and detector configuration. The three x-ray photon-object interactions are illustrated in this figure. One photon goes directly through the object and is recorded by the detector. A second photon is absorbed. These two phenomena lead to the contrast observed on a radiograph. The third photon is scattered at an angle to its original path. This photon, if recorded by the detector, yields no useful information about the object. In fact, it contributes "fog" or a background signal that degrades the quality of the projection. Consequently, focused collimators are used to prevent this scattered radiation from reaching the detector. They are made from an x-ray absorbing material such as lead and are focused back to the x-ray source for optimum collimation characteristics.

One of the chief advantages of tomography over conventional radiography is the greatly increased density resolution that can be achieved. Since, basically, tomography uses a series of radiographs taken at different angles, how is it possible to have higher density resolution than on the original radiographs? The following explanation will not prove this point but, hopefully, will give an appreciation of the basis of this fact. Consider the object shown in Figure 3(a) which consists of a solid material with a lower density inclusion C. Contours of radiographs taken at two different angles are shown at A and B. One of the techniques of computed tomography, to be considered in greater detail in a later section, is an iterative calculation of the absorption characteristics of the object that will make all of the radiographs taken at different angles self-consistent. For example, the signal on A produced by the x-ray transmission along path "a" must be consistent with the signal on B produced by the transmission along path "b." Since in an ordinary tomograph there are not just two but perhaps 180 views it can be seen that the self-consistency requirement will produce an increase in resolution of the object compared with that of a single radiograph. Consider now Figure 3(b) which has a region C' that has an absorption coefficient

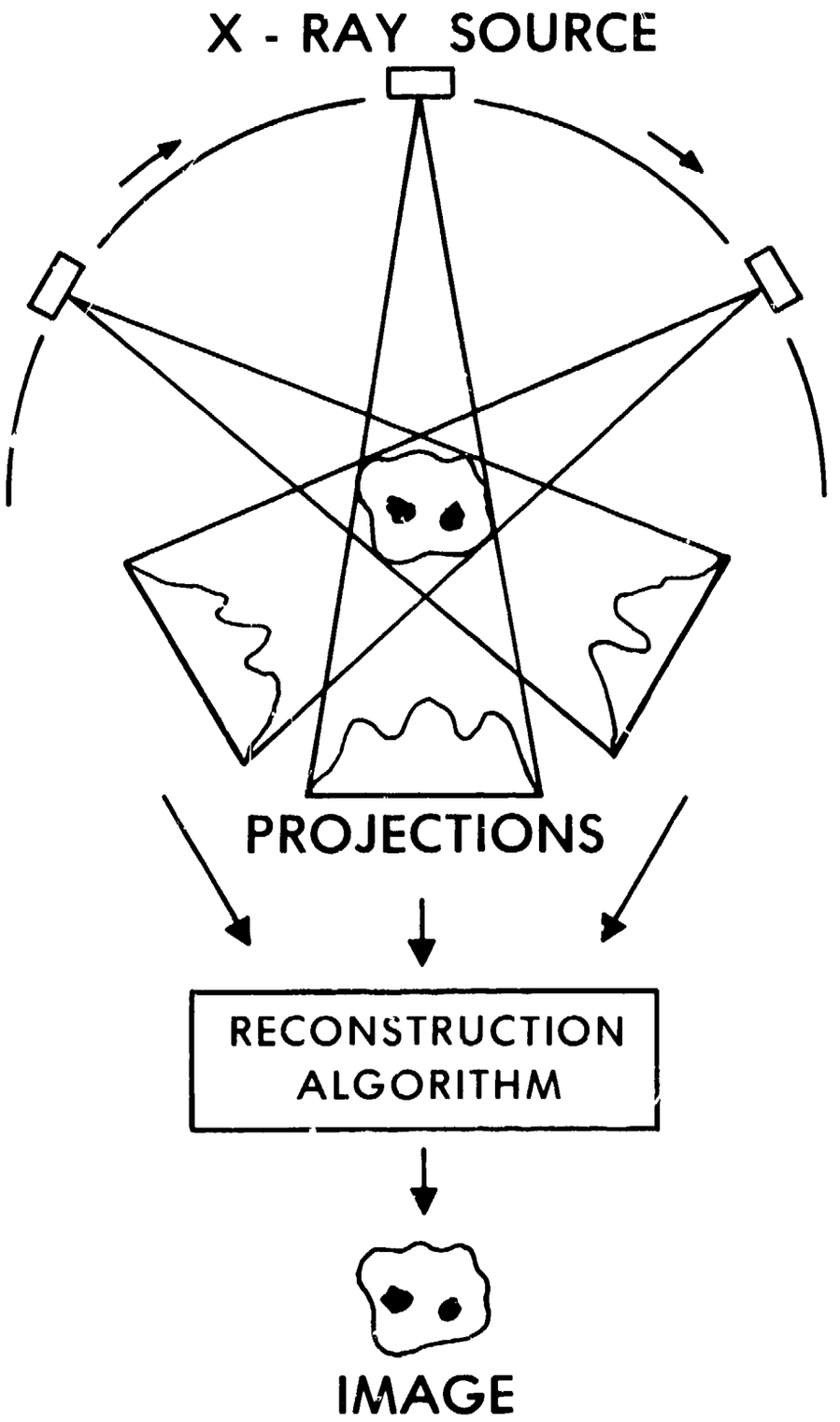

Figure 1. Typical Tomographic Configuration

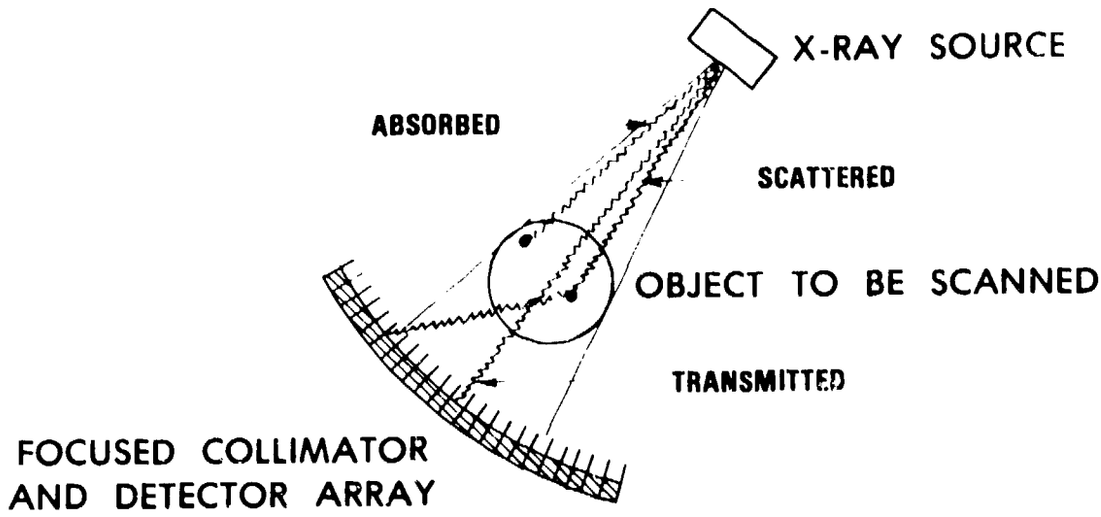

Figure 2. Source and Detector Arrangement

slightly less than the rest of the object and greater than inclusion C. The radiograph A' will have the same essential features as A. However, radiograph B' will be substantially different from B. The iterative reconstruction will then generate the object in Figure 3(b) which must have characteristics that will produce radiographs A' and B'. Thus, although A and A' are identical, the difference in B and B' contribute information in determining the properties of the object. In practical tomography, the 180 views require extensive iteration to yield self-consistent projections.

2.2 Theory of Reconstruction

2.2.1 General Ideas. X-ray radiation is attenuated when it traverses an object. The change in radiation intensity is given by

$$dI = -I\mu ds \quad , \tag{1}$$

where I is the intensity, ds is the path length, and μ is the proportionality constant or absorption coefficient. μ can depend on the energy of the x-ray as well as the composition of the material in each path length of the object. Solving the equation we get,

$$-\ln \frac{I}{I_o} = \int_o^x \mu ds \tag{2}$$

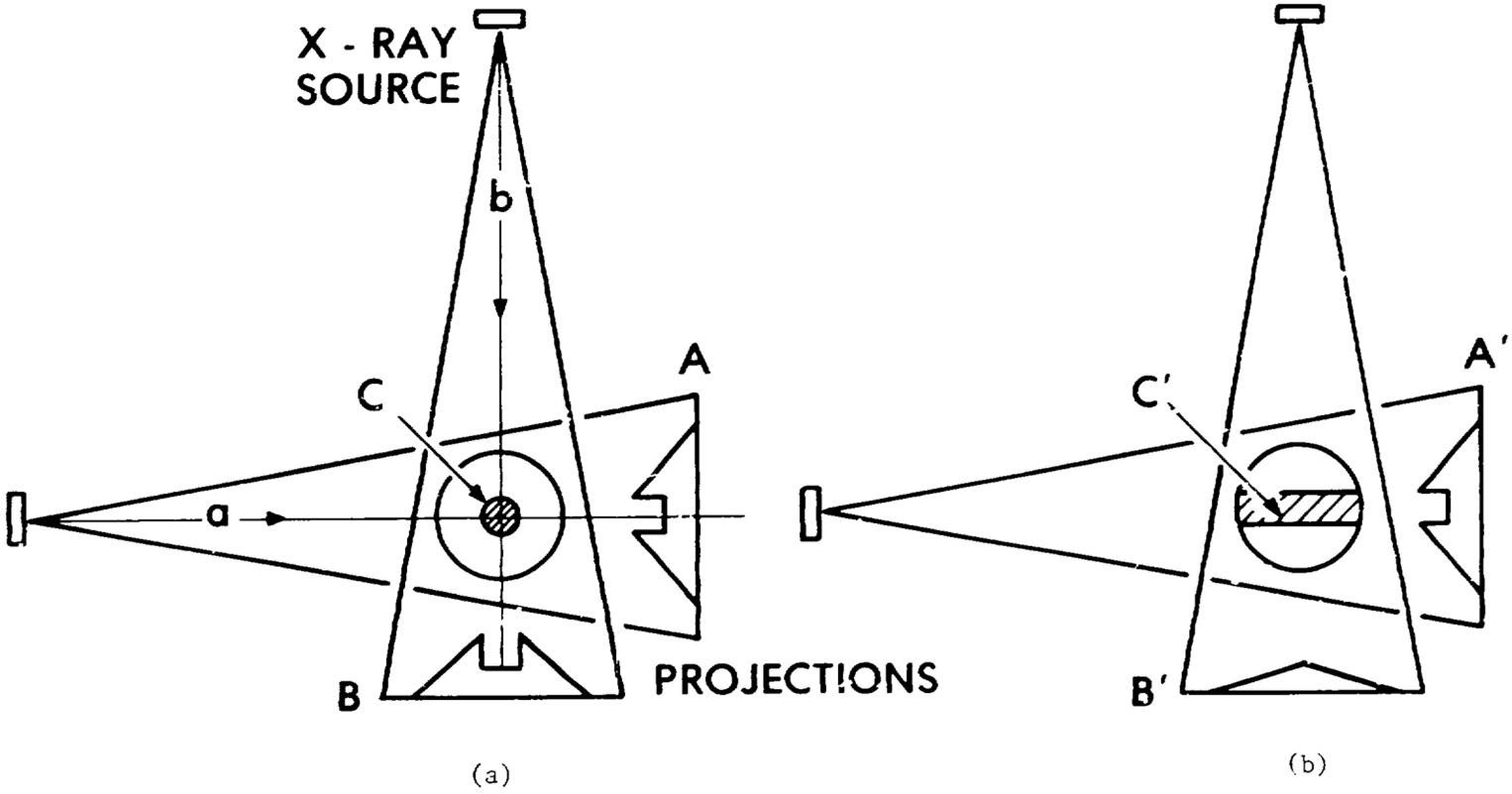

Figure 3. Sample Projections for Two Different Objects

where the integral is from the source to the detector. The x-ray shadowgraph or projection is a measure of I/I_o. The problem of tomography then, is to invert this equation and solve for μ of the object.

The density is deduced from the absorption coefficient by the relationship

$$\mu = \rho\sigma \tag{3}$$

when σ is the x-ray cross section of the material. These cross sections have been measured and calculated and depend on the x-ray energy and the atomic make-up of the material.

Computed tomography (CT) was made possible through an elegant mathematical proof by the Austrian mathematician Johann Radon[1] who in 1917 showed that an arbitrary function which is bounded, continuous and has continuous first partial derivatives can be uniquely reconstructed from an infinite set of parallel line integrals, such a those in Eq. (2). More generally then, one is interested in reconstructing an n-dimensional function, representing the value of a spatially distributed object, from its projections into an n-1 dimensional subspace. Assume that $f(\bar{s})$ defined only in the circular region $\bar{s}:\|\bar{s}\| < R$. Assume further that along lines L_i in R^n the values of the line integrals $g(L_i) = \int_{L_i} f(\bar{s})\, ds$ are known. The problem, then, is to estimate the value of $f(\bar{s})$ from the $g(L_i)$. Mathematically, this is equivalent to inverting the integral equation. Radon's exact solution, now called the inverse Radon transform, can be expressed as

$$f(\bar{s}) = \frac{1}{4\pi^2} \int_0^{2\pi} \int_{-\infty}^{\infty} \frac{-1}{t - x\cos\theta - y\sin\theta} \frac{\partial g(t,\theta)}{\partial t}\, dt\, d\theta \tag{4}$$

where $(t - x\cos\theta - y\sin\theta)$ is the perpendicular distance from $\bar{s}$ to the line $l(t,\theta)$ and $g(t,\theta)$ is the integral of $f(\bar{s})$ along the line $l(t,\theta)$. See Figure 4a.

To make these ideas clearer, suppose that one is interested in determining the two-dimensional density distribution $f(\bar{s})$, within a body. It is not possible to determine $f(\bar{s})$ directly, but, rather, it must be inferred from a set of external measurements. These are modeled as integrals of the absorption coefficient along rays in a plane through the object; such a ray in transmission tomography can be identified with a particular orientation of a highly collimated source and detector: The integrals are obtained by measuring the energy flux exiting the body along various paths, L_i, as in Eq. (2).

---

[1] *J. Radon, "Ueber die Bestimmung von Funktionen durch ihre Integralwerte laengs gewisser Manningfaltigkeiten," Berichte Saechsische Akad. Wiss., Vol. 69, pp. 262-277, 1917.*

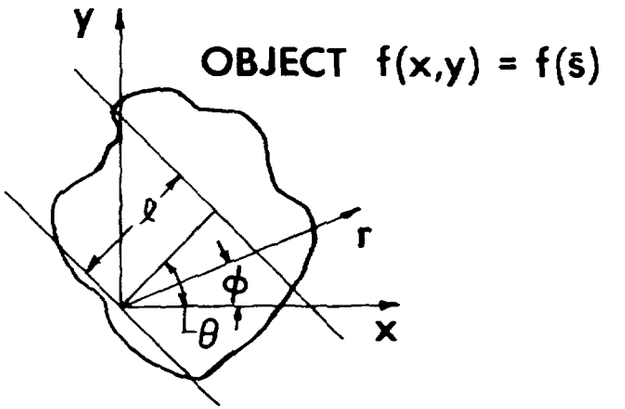

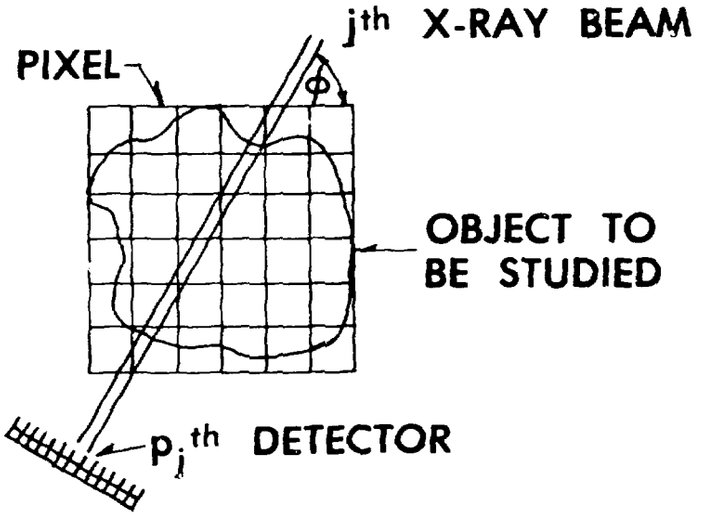

$\ell = x \cos\theta + y \sin\theta$

$\ell = r \cos(\theta - \phi)$

θ = NORMAL TO THE PROJECTION DIRECTION

ℓ = COORDINATE ALONG THE PROJECTION

(a) (b)

Figure 4. Reconstruction Geometry

A ray is defined parametrically by the relation $t = r\cos(\theta-\phi)$ and an ideal, i.e., noise-free measurement associated with the ray, taken at the angle θ, is defined by

$$g(t,\theta) = \iint_R f(t,\theta)\,\delta[t-r\cos(\theta-\phi)]\,|r|\,dr\,d\phi \qquad (5)$$

where $g(t,\theta)$ is the total x-ray absorption along the ray and the δ function exists only along the line of measurement, Figure 4b. The equation defines the measurement in terms of the unknown two-dimensional density. The reconstruction problem is to invert the measurements taken for a large number of rays to recover $f(t,\theta)$ throughout the disk R. That is, given measurements of the Radon transform

$$g(t,\theta) \text{ at } (t,\theta) \in A \qquad (6)$$

where A is the measurement set, determine an <u>estimate</u> of $f(\bar{s})$ for $\bar{s} \in B$, where B is the reconstruction set.

In practice the reconstruction is made difficult by the fact that only a finite number of line integrals are available and the data can be noisy. Thus, the basic assumptions of Radon's theory are not satisfied. One seeks algorithms which approximate Radon's transform in some sense. Three general approaches to the reconstruction problem have been developed: the series expansion, the convolution, and statistical algorithms. We will now discuss these briefly. The interested reader is also referred to Brooks and DiChiro,[2] Herman,[3] and the references cited therein.

The problem of reconstruction is approached by dividing the plane which contains the object of interest into equal sized picture elements, also called pixels. It is assumed that the x-ray attenuation in each pixel is constant. Thus, the object is represented by a two-dimensional array of numbers, typically a matrix of 256 x 256 (Figure 4). The measurements of x-ray attenuation along the rays then provides information on the total attenuation along a chosen line and known location.

For this feasibility study, we have examined three classes of reconstruction algorithms with the view to determine their degree of tolerance to missing information when only a limited number of views are available. In the following sections we summarize the basic ideas of each of these methods and give the relevant entries to the literature.

---

[2] *R.A. Brooks and G. DiChiro, "Principles of Computer Assisted Tomography (CAT) in Radiographic and Radioisotopic Imaging," <u>Phys. Med. Biology</u>, Vol. 21, No. 5, pp. 689-732, 1976.*

[3] *G. Herman, <u>Image Reconstruction from Projections</u>, Academic Press, New York, 1980.*

2.2.2 Series Expansion Methods. In the series expansion algorithm, the function $f(\bar{s})$ is approximated by a finite number of terms in a series expansion on a known basis set. This problem formulation leads to a matrix problem which can be solved by a number of different techniques, such as numerical relaxation used by Gordon[4] and Herman,[5] for example, in the Algebraic Reconstruction Technique (ART) family of algorithms.

This method proceeds from the idea that a picture of the object under study can always be represented by a linear combination of a fixed set of basis pictures. The reconstruction problem is then one of estimating an N-dimensional column vector whose i-th component is the coefficient of the i-th basis picture in the linear combination. A good choice of the basis function, $b_j(r,\phi)$ is to assure it to have a value of one if (r,ϕ) is inside the j-th pixel, and zero outside.

The problem is then one of finding a function whose integrals over a given domain match the measured values. The object to be reconstructed is now subdivided into pixels (Figure 4(b)), each of which is assigned a value of the unknown function f_i. The radiation, after it traverses the object through the beam j, is detected at the detector element p_j. The line integral, Eq. (2), is then estimated as a sum of its values in the pixels along the ray path.

The calculation commences by assuming a value for the function f_i and calculating the projection p_j along the ray path. If the ray sum is not equal to the projection values, the value of the cell that contributes to the ray sum is changed by an appropriate amount and the calculation is repeated for all cells and rays. The iteration is continued until the desired accuracy is obtained.

Iterative algorithms are more tolerant to missing data,[2] but overall give less accurate results than some of the newer algorithms. The reason for the inaccuracy can be found in the fact that here one attempts to find a function which is piecewise constant on the pixels. Also, the x-ray beam is represented by a strip of finit width instead of a line.

There are several other drawbacks to the series expansion technique. First, one needs all the projection data before a reconstruction can be commenced and, also, it requires more operations than other algorithms. Further, iterative reconstructions are more susceptible to errors caused by noise in the data.

A decided advantage of this type of approach is that it can be used to generate reasonable results when data is missing, such as in the case of limited number of angles and limited view of the object of reconstruction.

---

[4] *R. Gordon, "A Tutorial on ART," IEEE Transactions on Nuclear Science, NS-21, pp. 78-93, 1974.*

[5] *G. Herman, "ART: Mathematics and Applications," J. Theor. Biology, Vol. 42, pp. 1-32, 1973.*

This is quite an important consideration for the application of tomography for transient phenomena.

2.2.3 Convolutional Algorithm. The other large class of reconstruction methods comes under the heading of convolutional algorithms.[6, 7] In such an approach, one obtains the density estimate by applying a linear mapping to the set of measurements. A number of different algorithms can be derived based on these ideas depending on the choice of the weight functions or filters used in these mappings. The steps of the algorithm are

a) at each value of θ_k, filter the measurement $g(t,\theta_k)$ to obtain $s(t,\theta_k)$,

b) back project $s(t,\theta_k)$ as a constant along all points of $\underline{x}$ on each line, t,

c) add the projections over k = 0, . . . K

Note that without a filter function, a blurred image is obtained due to the unavoidable contribution from each back projected profile to the area around the object. Filtering introduces negative values into the profile that cancel out undesired components in the field image. The process of multiplying the values of each profile by a set of values, the filter function, is called a convolution; hence, the name convolved filtered back projection is sometimes used. Back projected images are sensitive to a reduction of the available amount of data with the result of the appearance of artifacts. Also, noise in the data can produce a mottled appearance because high frequency components in the projected data are emphasized, leading to computational errors.

2.2.4 Maximum Entropy Image Reconstruction. In communication theory information has the same mathematical form as that of entropy in thermodynamics or statistical mechanics. They both express the logarithm of the number of possible messages or the number of possible states in a given system.

By the second law of thermodynamics, it is known that a system left to itself will evolve in a certain direction and entropy gives an indication of the direction and stage of the process. Equilibrium is reached when the entropy reaches a maximum. In statistical mechanics entropy can be given a probabilistic meaning which makes a direct comparison between the concepts of information and entropy possible.

---

[6] *L.A. Shepp and J.B. Kruskal, "Computerized Tomography: The New Medical X-Ray Technology," Amer. Mathematical Monthly, Vol. 85, pp. 420-439, 1977.*

[7] *R.N. Bracewell and A.C. Riddle, "Inversion of Fan Beam Scans in Radio Astronomy," Astrophys. J., Vol. 150, pp. 427-434, 1967.*

Entropy is then defined as $S = k\ell nP$ where P are the number of equally probable microscopic states of the system and k is the Boltzmann constant. The definition can be generalized somewhat if not all states are equally probable to the following form $S = -k\Sigma p_i \ell n p_i$ with $\Sigma p_i = 1$ where p_i is the probability that the system is in state i.

In the communication theory usage of the concept, entropy has to be reinterpreted somewhat. A measure of information could be, for example, a monotonic function of the number of messages in a set from which a particular message is selected. The log of this function is used because it makes the information a linear quantity proportional to such characteristics as duration of the message or the number of communication channels. Thus, information in a message is usually defined as $I = k\ell nP$ where k is the constant and P the number of messages in a set of equally probable messages from which a particular one has been selected.

Recalling the observation of Boltzmann that entropy is a measure of missing information and noting that a reconstructed image free of artifacts should contain less information than one with artifacts, the notion of maximizing the entropy of a reconstruction suggests itself.

To make the connection between the notions of communication theory and actual x-ray absorption measurements, consider an object to be described by M parameters $(f_1, f_2, \ldots f_M)$ each of which could represent a sample of the object, $f_i = f(x_i, y_i)$. Since the number of measurements needed to adequately describe an object is usually much greater than the actual number of measurements taken, the object is underdetermined leading to an infinite possible number of descriptions of the object. To make the system determinate constraints are imposed such as an entropy criterion leading to a constrained optimization problem. The connection between the P_i and actual observables can be made by considering the object to be partitioned into N pixels each of uniform area a. Let f_i be the attenuation of an x-ray in the i-th pixel. Now

$$f_i = \frac{E}{a} r_i$$

where E is the energy of a photon, r_i the rate of absorption in the i-th pixel. Then the probability that a photon is absorbed in the i-th pixel is

$$P_i = \frac{r_i}{\sum_i r_i} \tag{7}$$

The entropy of the discrete probability distribution then becomes

$$S = -\sum_{i=1}^{N} P_i \ell n P_i \quad . \tag{8}$$

Minerbo,[8] noting that the source function obeys

$$f(x,y) \geq D \tag{9}$$

$$\int dx \int_D f(x,y)\, dy = 1 \tag{10}$$

where D is the compact support, observed that the function f can now be regarded as a probability distribution. If projection data are available as

$$G_{jm} = \int_{S_{jm}}^{S_{im}+1} ds \int_{-\infty}^{\infty} f(s\cos\theta_j - t\sin\theta_j,\ s\sin\theta_j + t\cos\theta_j)\, dt \tag{11}$$

$$m = 1,\ldots M(j)$$
$$j = 1,\ldots J$$

where θ_i are the projection angles and S_{ji} are the abscissas for the j-th view. Of course, $G_{jm} \geq 0$ and $\sum_{m=1}^{M(j)} G_{jm} = 1$. Minerbo then proceeds to define the entropy of f as

$$\eta(f) = -\int dx \int_D f(x,y)\, \ell n\, [f(x,y)A]\, dy \quad \text{where} \tag{12}$$

A is the area of D. Next, Lagrange multipliers are introduced for each of the constraints and Lagrangians are formed. The standard procedure is concluded by using a nonlinear Gauss-Seidel technique to solve the system of equations.

The MENT technique has been used with some success for reconstruction of objects and seems to yield smoother images than the filtered back projection or the ART family of algorithms when the number of views is restricted.

3. BALLISTIC REQUIREMENTS

3.1 The Ballistic Environment

The ballistic environment imposes rather severe constraints on the system under consideration. These can be summarized as follows: The time constant of a typical phenomenon inside a gun tube, for example, is of the order of tens of microseconds while typical length scales are around a millimetre. To

[8] *G. Minerbo, "MENT: A Maximum Entropy Algorithm for Reconstructing a Source from Projection Data," Computer Graphics and Image Processing, Vol. 10, pp. 48-68, 1979.*

avoid blurring in the reconstructed images due to motion, all the transmission measurements will have to be taken in a few tens of microseconds. Thus, for a ballistic application, there is no time to move the source to succeeding locations but rather, an arrangement must be considered whereby the data is gathered by flashing a number of sources in a short time interval. With the high cost of each additional source in mind, as well as the difficulties of sequencing the flashes and recording the results, it is desirable to minimize the number of views; i.e., the number of sources required for a system. Therefore, one of the basic questions that this study sought to answer was: What is the least number of sources that are necessary for a reconstruction consistent with a resolution of the image of the order of millimetres?

Due to the high pressures and temperatures of the operating environment, special attention must be given to protecting the recording equipment in the experiments. Pressure of the order of several hundred atmospheres and temperatures of around 3000 K are not uncommon. The differences between the medical and ballistic application are summarized in Table 1.

3.2 Special Aspects of Ballistic Tomography

3.2.1 Materials of Interest. Tomography on real gun tubes is made difficult by the fact that the x-ray signal has to traverse several centimetres of highly absorbing steel. To obtain a sufficient detector signal for reconstruction, high energy x-rays are needed. Such equipment becomes rather bulky and difficult to operate. In addition, the hydrocarbon propellant material within the chamber is of a much lower density and has a lower absorption coefficient than the steel walls, leading to problems with contrast on the x-ray projections.

This difficulty has been overcome by Hornemann,[9] who used a polyamid fiber reinforced plastic (Kevlar) tube to study propellant grain motion under conditions approximating an actual firing of a 20-mm gun system. The tube could withstand pressures up to 200 MPa when the wall thickness was 10 mm, and was transparent to 120 kV flash x-ray source pulses. Large caliber investigations on the ignition and early combustion phase in 155-mm and 5-inch cannons have been carried out using filament-wound fiberglass tubing with a wall thickness of 3 to 4 mm.[10-12] The x-ray sources used were 300 kV and

---

[9] *U. Hornemann, "Investigation of Propellant Combustion in X-Ray Transparent Gun Tubes," Ernst-Mach-Institut/Abteilung fuer Ballistik Report No. 3/79, Weil am Rhein, West Germany, 1979.*

[10] *T.C. Minor, "Characterization of Ignition Systems for Bagged Artillery Charges," ARBRL-TR-02377, USA ARRADCOM/Ballistic Research Laboratory, Aberdeen Proving Ground, MD, 1981 (AD A108119).*

[11] *A.W. Horst and T.C. Minor, "Ignition Induced Flow Dynamics in Bagged Charge Artillery," ARBRL-TR-02257, USA ARRADCOM/Ballistic Research Laboratory, Aberdeen Proving Ground, MD, 1980 (AD A090681).*

[12] *W.R. Burrell and J.L. East, "Effects of Production Packing Depth and Ignition Techniques on Propelling Charge Reaction and Projectile Response," NSWC/DC TR-3705, Naval Surface Weapons Center, Dahlgren, VA, 1979.*

TABLE 1. COMPARISON OF MEDICAL AND BALLISTIC REQUIREMENTS

	Medical	Ballistic
Time	2-5 s	1-100 μs
Spatial Resolution	<1 mm	Several mm
Temperature	Ambient	3000 K
Pressure	Ambient	1-300 MPa (Blast)
Number of Views	180	~20
Contrast	Bone-Tissue	Hydrocarbon
Scattering	1 View	20 Views
Dynamic Range Requirement	10^8	10^2

450kV. The maximum pressure obtained in these experiments is approximately 70 MPa. Other materials with minimum absorbing x-ray properties are available. As shown in Table 2, several of these materials are as strong as steel. One drawback to their use is that at elevated temperatures they lose their tensile strength; thus, they cannot be used for cyclic firing.

3.2.2 Radiation Transport Calculations. A useful assessment of these materials as chambers for ballistic investigation can be carried out by doing radiation transport calculations on a propellant-chamber mock-up. A one-dimensional Monte Carlo code, TIGER, developed by the Sandia Laboratories,[13] was used to carry out the transport calculations. From 1000 to 50,000 photon histories were followed with the code. Mono-energetic x-rays were used as input. The chamber propellant configuration is shown in Figure 5. A monolithic propellant grain is used to simulate the granular propellant bed, with a thickness (124 mm) equivalent to that found in a relatively high loading density configuration. Using the known geometry, density, and chemical composition of the object, the code calculates the percentage of energy absorbed, forward-scattered, back-scattered and unattenuated within the object material. The output also includes the percentage of photons absorbed, forward-scattered, back-scattered and unattenuated, and the energy distribution of the scattered photons. Scattered radiation is defined as all radiation transmitted through the object with a different energy than the

[13] *J.A. Halbleib and W.H. Vandevender, "TIGER: A One-Dimensional Multilayer Electron/Photon Monte Carlo Transport Code," SLA-73-1026, Sandia Laboratories, Albuquerque, NM, 1974.*

input radiation. An example of this output is given in Figure 6, in which the chamber was made of fiberglass. This is a one-dimensional code and does not give an angular distribution of the scattered radiation but only an energy distribution. Table 3 gives the results for a fiberglass and a steel chamber with input x-ray beams of 0.1 MeV up to 1.0 MeV for the unattenuated and

TABLE 2. COMPARISON OF TYPICAL MATERIAL PROPERTIES

Material	Density g/cm^3	Tensile Strength GPa	Tensile Modulus GPa
Steel	7.75	1.38	200
S-glass/epoxy	2.08	1.66	48
Kevlar/epoxy	1.38	1.38	76
Carbon fiber/epoxy	1.55	1.38	124

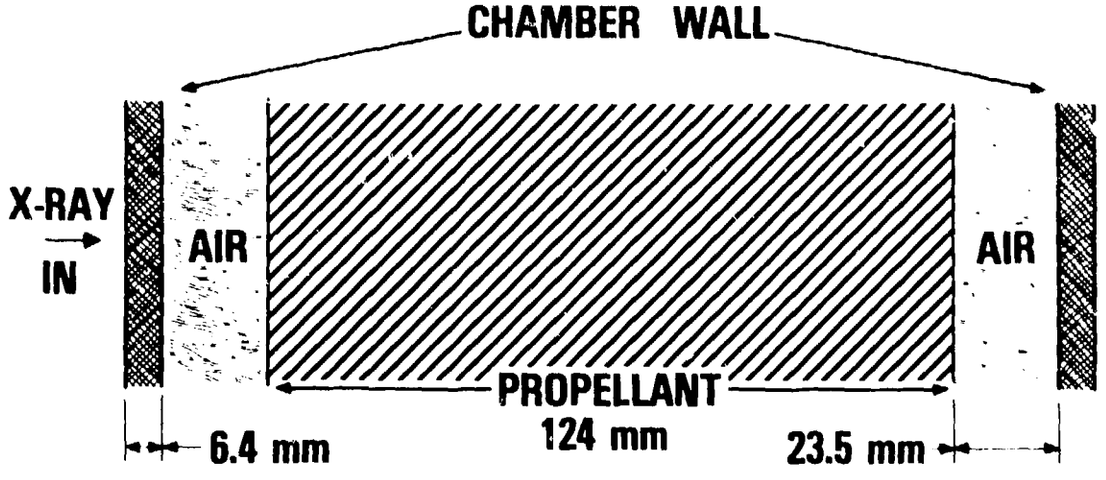

Figure 5. Propellant-Chamber Mock-Up for X-Ray Transport Calculations

TABLE 3. RESULTS OF THE MONTE CARLO CALCULATION OF X-RAY INTERACTION WITH 155-MM CHAMBER SIMULATOR*

Chamber Wall Composition	X-Ray Energy (MeV)	Percent Energy Unattenuated	Percent Energy Forward Scattered	Percent Photons Unattenuated	Percent Photons Forward Scattered
Fiberglass	0.1	3.4	10	3.4	15
	0.25	7.7	16	7.7	28
	0.5	14	18	14	37
	1.0	24	18	24	38
Fe	0.1	0.4	0.3	0.4	0.3
	0.25	9.7	15	9.7	28
	1.0	24	18	24	34

*See Figure 5 for configuration.

forward-scattered radiation. The presence of forward-scattered radiation in a radiograph is undesirable as it contributes fog or background noise to the signal. In addition, the percentage of energy transmitted is also important since this determines the strength of the signal from the detector. Hence, in the absence of the knowledge of the angular distribution of the scattered radiation, a useful quantity to consider is the ratio of unattenuated to forward-scattered radiation. It is clear from Table 3 that the high energy x-rays are superior, whether the chamber is made of steel or fiberglass. As will be discussed in Section 4.2, the x-ray sources under consideration are poly-chromatic and are similar to those used in References 9 through 12. Further tests must be carried out to determine the significance of radiation below 0.1 keV on the quality of these radiographs.

Results for calculations at 0.1, 0.25, 0.5, and 1.0 MeV are given in Figures 7 (steel chamber) and Figure 8 (fiberglass chamber). A low energy x-ray filter, such as copper or aluminum, could be used between the object and the detector. Calculations must be done to determine the amount of scattered radiation that would be contributed from these filters themselves. These figures show an apparent anomaly between the absorbed energy and the absorbed photon fraction. This is because the scattered x-ray photons are in lower energy bins than the incoming radiation. To conserve energy, the remainder of the energy of the scattered photons is lost through absorption. It is worth noting that above 0.25 MeV there is little difference between the steel and fiberglass chambers. This is not surprising since the dominant path length is through propellant in this thin-walled chamber configuration. At 0.1 MeV,

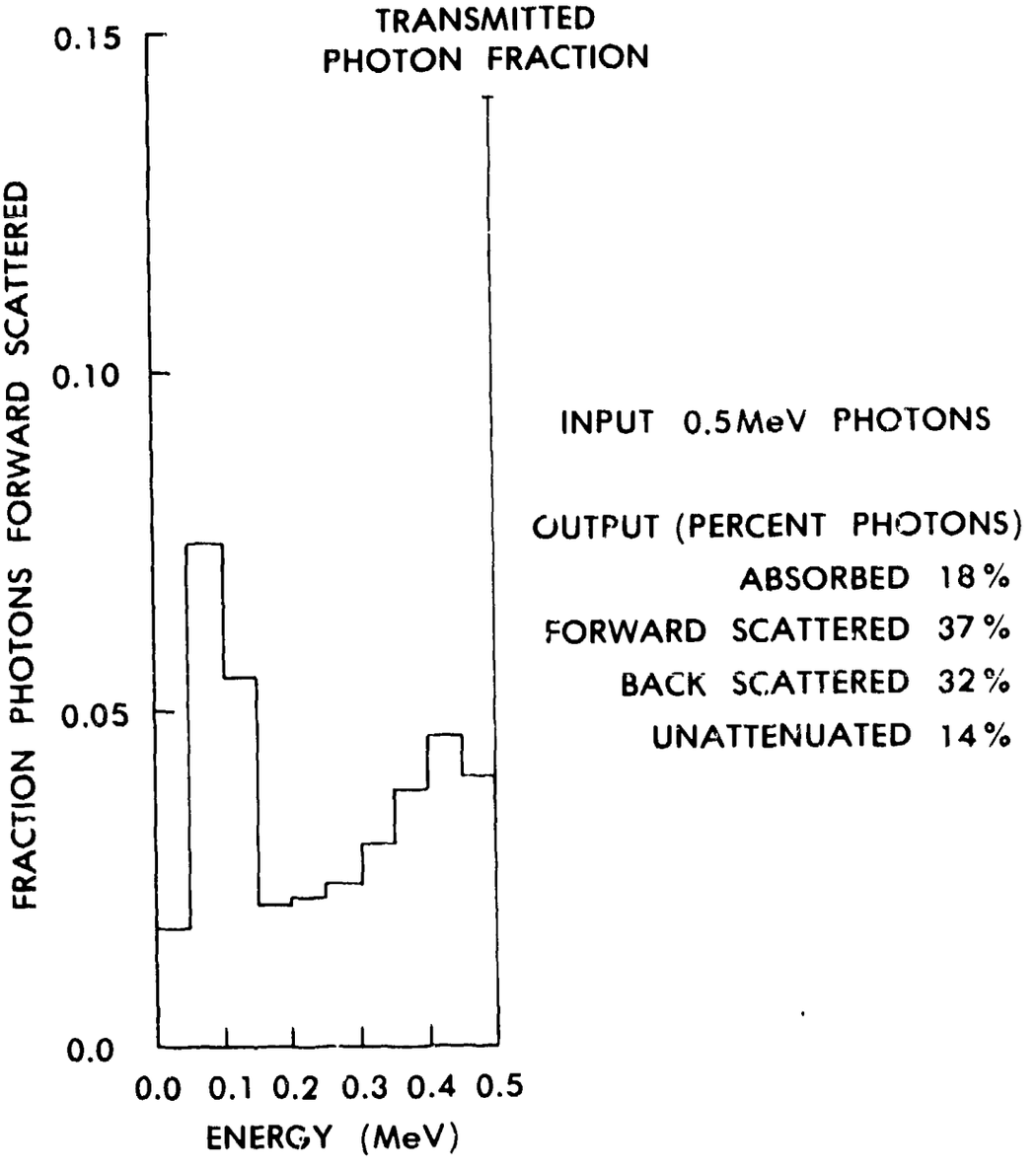

Figure 6. 0.5 MeV X-Ray Transport Calculations

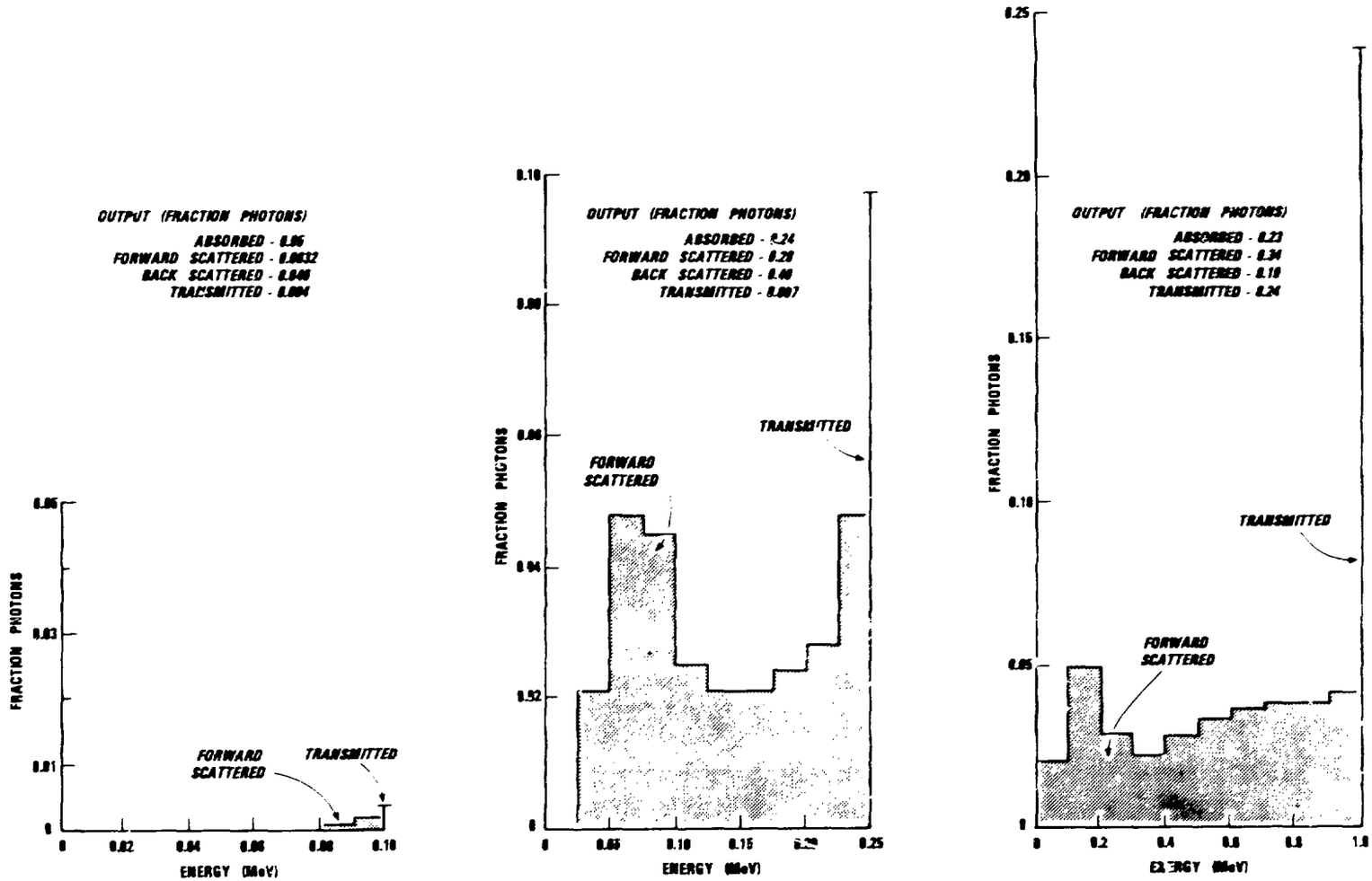

Figure 7. Steel Chamber: Transport Calculations for 0.1, 0.25, and 1.0 MeV X-Rays

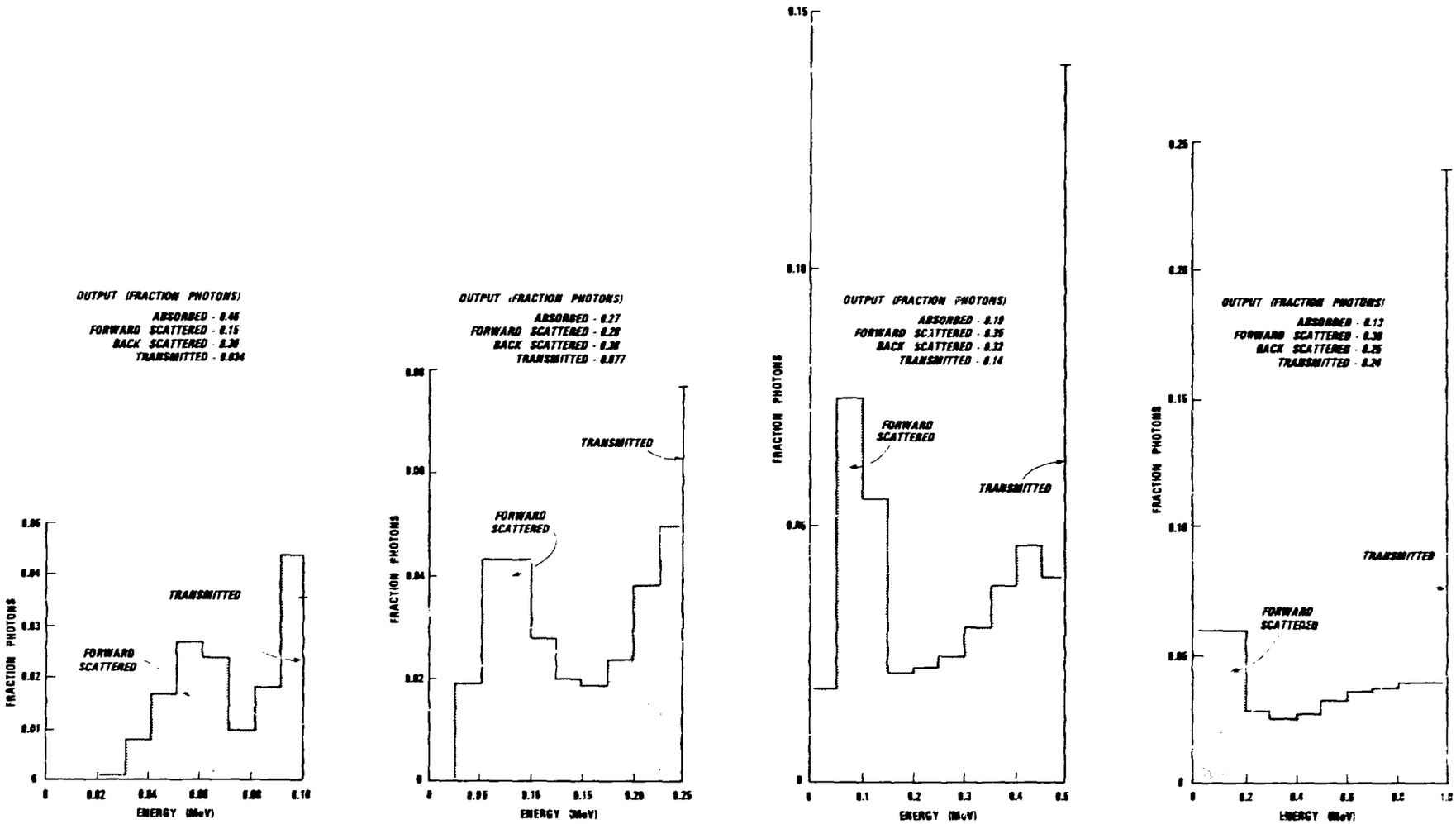

Figure 8. Fiberglass Chamber: Transport Calculations for 0.1, 0.25, 0.5, and 1.0 MeV X-Rays

Table 3 shows that the unattenuated-to-forward scattered ratio is more favorable for the steel chamber. However, the transmitted radiation is an order of magnitude lower which may be too small to produce acceptable radiographs.

Calculations were carried out on the actual 155-mm howitzer chamber configuration, in which the wall was 71-mm thick steel. 1.0-MeV x-rays are too soft for this application with less than 0.1% transmission. Results for 5.0-MeV x-rays are shown in Figure 9. It is seen that most of the scattered radiation is between 0 and 1.5 MeV. The ratio of unattenuated-to-forward scattered photons is reasonably good at 5.0 MeV. Broz[14] has carried out an experimental investigation on gun tubes with a 2.3 MeV flash x-ray unit. Acceptable radiographs through 99 mm of steel were made using this system.

In summary, it appears that high energy x-rays (5.0 MeV) would be needed to acquire the projections of radiographs adequate for tomographic reconsruction, when examining an actual 155-mm cannon. However, using a thin-walled chamber of either steel or fiberglass, the calculations show that x-ray energies between 0.1 and 1 MeV should give a reasonable amount of transmitted radiation.

Detectability is not the only concern here. Will there be enough contrast in the image to produce signals with an adequate signal-to-noise ratio? The propellant-chamber configuration does not vary greatly in density unless there are large void spaces within the propellant bed. To obtain some idea of image contrast, calculations were carried out with the configuration of Figure 5 with two propellant thicknesses, 124 mm and 114 mm. This simulates an arbitrary ten percent change in propellant loading within the chamber. Results of calculations using a fiberglass and a steel chamber for 0.1 and 0.5 MeV are shown in Table 4. A summary of this table and the calculated contrast is shown in Table 5. No attempt has been made to assess the importance of scattered radiation on the contrast. There are errors inherent in the calculations and the contrast numbers should only be considered an order of magnitude. A more straightforward calculation using standard absorption coefficients could have been used but the TIGER code includes the scattered component as well. Table 4 indicates that no unexpected results due to scattering were observed.

3.2.3 Limited Number of Views. Due to the constraints discussed in Section 2.1, it is desirable to limit the number of sources, and, consequently, the number of views which will be available for a reconstruction. But the fewer the views the less information is available and the more likely that artifacts in the form of streaks will appear in the reconstructed image. The distance between the streak and the object is a function of the number of views and the spatial resolution.

Since in medical diagnostics there was little incentive to minimize the number of views, only a few authors even comment on this problem. To

[14] *A.L. Broz, "Methodology Investigation of Techniques for In-Bore Flash Radiography," TECOM Project No. 7-CO-PB5-AP1-086, Material Testing Directorate, Aberdeen Proving Ground, MD, 1977 (AD B0228342).*

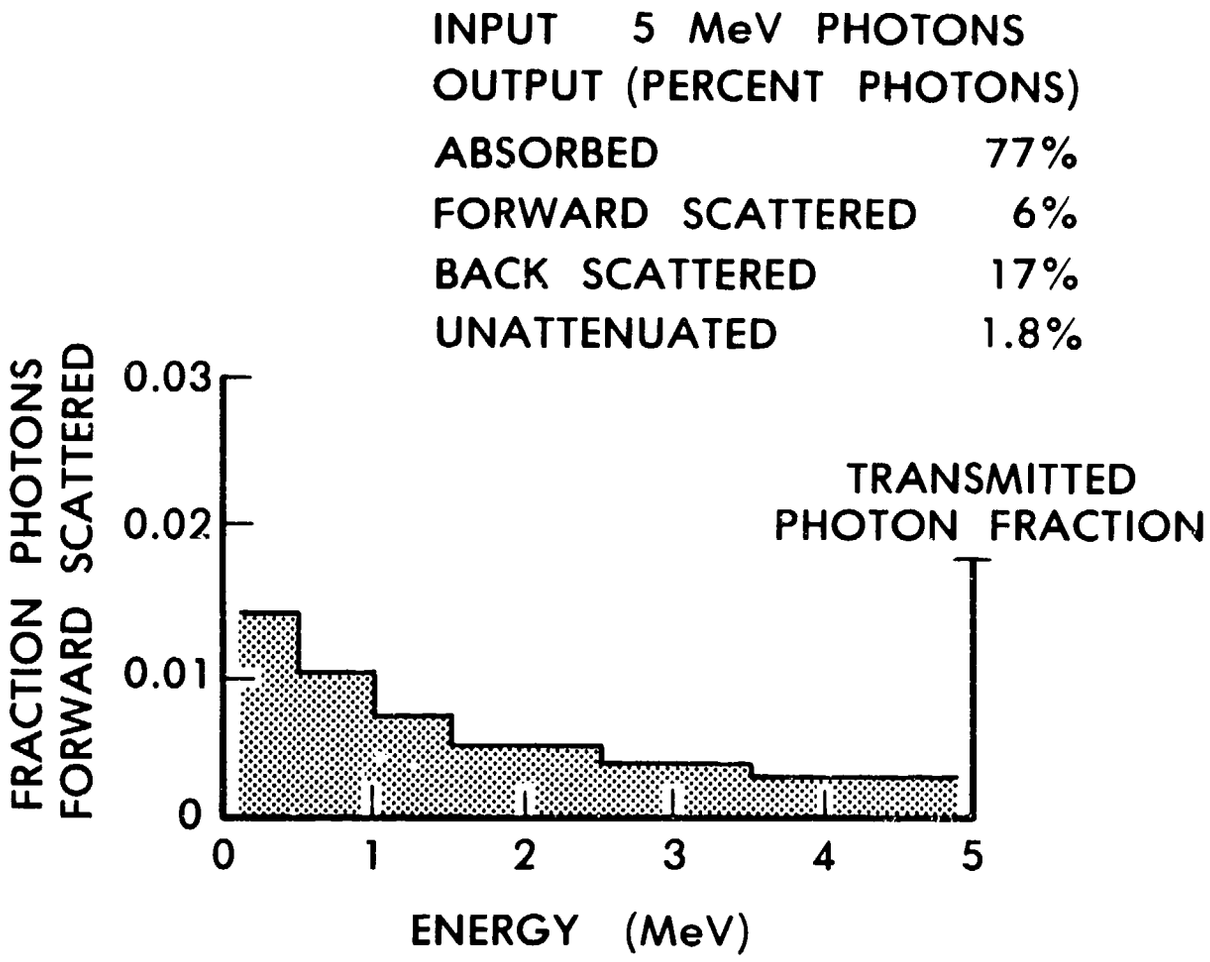

Figure 9. Transport Calculations for 5 MeV X-Rays for Actual 155-mm Chamber

TABLE 4. RADIATION TRANSPORT CALCULATION

PROPELLANT THICKNESS (MM)	INPUT ENERGY (MeV)	NUMBER OF PHOTONS (%)				PHOTON ENERGY (%)			
		UNSCATTERED	FORWARD SCATTERED	BACK SCATTERED	ATTENUATED	UNSCATTERED	FORWARD SCATTERED	BACK SCATTERED	ATTENUATED
FIBERGLASS CHAMBER									
114	0.1	4.6	16	36	42	4.6	12	24	59
124	0.1	3.2	14	36	47	3.2	10	24	63
114	0.5	16	37	31	15	16	20	9	55
124	0.5	14	35	33	18	14	18	9.3	59
STEEL CHAMBER									
114	0.1	0.27	0.33	4.1	95	0.27	0.30	3.1	96
124	0.1	0.25	0.23	4.4	95	0.25	0.21	3.3	96
114	0.5	9.3	19	18	54	9.3	13	6.1	72
124	0.5	7.7	18	18	57	7.7	12	6.3	75

TABLE 5. X-RAY CONTRAST CALCULATIONS

Chamber*	Energy (MeV)	Propellant Thickness (mm)	Photon Unscattered (%)	Contrast** (%)
Fiberglass	0.1	114	4.6	19
Fiberglass	0.1	124	3.2	
Fiberglass	0.5	114	16	14
Fiberglass	0.5	124	14	
Steel	0.1	114	0.27	8
Steel	0.1	124	0.25	
Steel	0.5	114	9.3	20
Steel	0.5	124	7.7	

Configuration shown in Figure 5

***Contrast calculated as the percent change in unscattered photons in going from 114 to 124 mm propellant.*

determine the least number of views for an acceptable reconstruction, Snyder and Cox[15] give the formula $N = \pi v_o$ while later Joseph and Schulz[16] proposed

$$N = 2\pi \frac{Dv_o}{(1-\sin\frac{\psi}{2})} \qquad (13)$$

where N is the minimum number of views, D the maximum object diameter, v_o the maximum resolvable spatial frequency and ψ the opening angle of the fan. Experience with these equations shows that the results which they give are only reliable if one assumes the number of views and calculates D. In fact,

[15] *D.L. Snyder and J.R. Cox, "An Overview of Reconstructive Tomography and Limitation Imposed by a Finite Number of Projections," in Reconstruction Tomography in Diagnostic Radiology and Nuclear Medicine, M.M. Ter Pogossian, et al, editors, University Park Press, Baltimore, MD, 1977.*

[16] *D.M. Joseph and R.A. Schulz, "View Sampling Requirements in Fan Beam Computed Tomography," Med. Phys., Vol. 7, No. 11, 1980.*

it is more reasonable to interpret D, not as the diameter of the object but the distance at which an artifact appears from a sharp edged object.

Without giving details, K.T. Smith, et al,[17] report on reconstructions of a pig's head phantom using 18 x-ray directions. Density variations without obscuring artifacts are clearly visible.

Finally, the paper by Crowther, et al.[18], should be mentioned. It states that the minimum number of views, N, to reconstruct a particle of diameter D to a resolution of d is given by

$$N \approx \pi D/d \quad . \tag{14}$$

More quantitative research is needed before the least number of views question can be answered with any degree of certainty. An effort to determine the minimum number of views for the ballistic application is described in Section 4.

4. RESULTS OF STATIC EXPERIMENTS

Early in the study it was realized that a limited number of static experiments would be useful in helping to establish the feasibility of building a tomographic system for ballistic applications. The experiments were designed to answer the question on the least number of sources that could be used for an acceptable reconstruction and whether sufficient contrast could be obtained from x-ray sources in the sub-MeV regime. As it turned out, both of these questions could be answered in an acceptable manner. The experiments were performed at the Los Alamos National Laboratory. The experimental set-up[19] consisted of a source, a detector, a rotating table, and ancillary electronics required for the subsequent data reduction. See Figure 10.

The source was Iridium with most γ-radiation at 316 keV and 468 keV. The beam was collimated to a cone with a 2 cm diameter base at the detector. The source to detector distance was 0.6 m. A detector consisting of a NaI(Tl) scintillator fronting a single photomultiplier tube was used to record the

---

[17] *K.T. Smith, D.C. Solman, and S.L. Wagner, "Practical and Mathematical Aspects of the Problem of Reconstructing Objects from Radiographs," Bulletin of the American Math. Society, Vol. 83, pp. 1227-1270, 1977.*

[18] *R.A. Crowther, D.J. DeRosier, and A. Klug, "The Reconstruction of a Three-Dimensional Structure from Projections and Its Applications to Electron Microscopy," Proc. Royal Society London, Vol. A317, pp. 319-340, 1910.*

[19] *R.P. Kruger, "Nonmedical Applications of Computer Tomography to Power Capacitor Quality Assessment," IEEE Transactions on Nuclear Science, NS-28, pp. 1721-1725, 1981.*

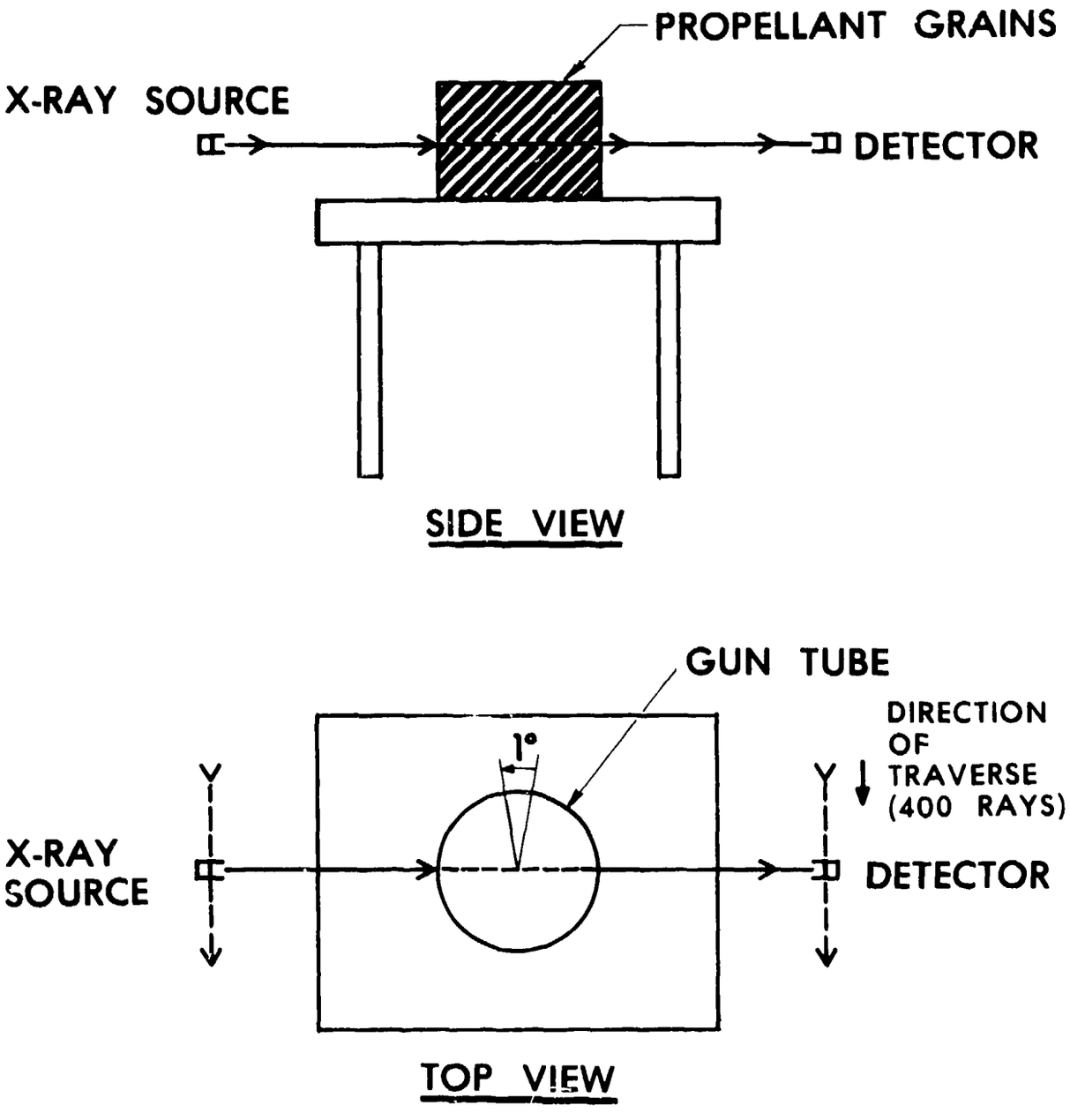

Figure 10. The LANL Experimental Setup

transmitted radiation. It was placed behind a detector collimator having movable plates which permits the collimator aperture to be varied in size from 0.5 mm up to several millimetres on a side. A 12-bit analog to digital converter with a 40 μs digitizing time was used for the recording of the x-ray transmission through the object. The study module was placed on a table allowing three degrees of freedom of motion. The axes were driven by direct current stepping motors controlled by an LSI-11 computer. The projection data was recorded on floppy disks.

The experiments were performed on two different test phantoms. In the first, a 20.0 cm diameter fiberglass cylindrical tube, with a wall thickness of 3 mm was filled with inert, 7-perforation (diameter 1 mm) propellant grains, of 1.0 cm in diameter and 2.0 cm in length. This material contained 31 percent Pb_3O_4. For the second test, the test pellets, the same size as before but now consisting of lucite, were embedded in a styrofoam matrix and oriented at random angles (Figure 11c). This approximates the fluidized regime within a gun tube. In both cases, x-ray absorption measurements were made with 800 data points per view angle and the experiment was repeated 180 times, stepped at one-degree intervals. The scan aperture was 0.5 mm by 1 mm and the step over between samples was 0.25 mm. It took approximately six hours to acquire the data for one reconstruction. This was the basic data set used in the reconstructions.

With the data in hand, using the MENT and a filtered back projection (FBP) codes, computer experimentation was begun. The objective was both to determine the quality of the reconstructed image when data points were intentionally omitted and when fewer than 180 views were used. Indeed, the question we sought to answer was: What is the least number of views which will allow a reasonable tomographic reconstruction to be obtained?

The result of the study is illustrated in Figures 11a through 11i. In (a), the first phantom was reconstructed with the filtered back projection using 180 views and 400 points per view angle. Thirty-six views were used for the reconstruction shown in (b). Note that the artifacts become discernible and detail is lost. The second phantom is shown in (c) with a 180-view FBP reconstruction in (d) and an eighteen-view reconstruction (e). When the reconstruction is performed using MENT for the same number of views and two hundred points, the image seen in (f) exhibits fewer artifacts. Finally, in (g) nine views were used and the results show the clustering of the propellant grains and the general topology of the flow but quantitative evaluation is no longer feasible. Further analysis of the experimental data was carried out for the purpose to be discussed in Sections 5.2 and 6. Reconstructions were done when only 100 (h), 50 (i), and 25 sets of data points per view were used. Below 50 data points, the fuzziness of the obtained picture precludes any quantitative use of the results. We conclude from this that the reconstructed picture definition is determined by the number of projections (18) rather that the number of points per projection.

It is possible that another algorithm may yet be devised which would allow a reconstruction yielding reliable quantitative data at or below nine views. An effort in this direction is on the way. However, at present, between 15 and 20 views represent the lower bound of usefulness of these techniques with MENT conferring the advantage of fewer artifacts and a smoother picture for the restricted data set.

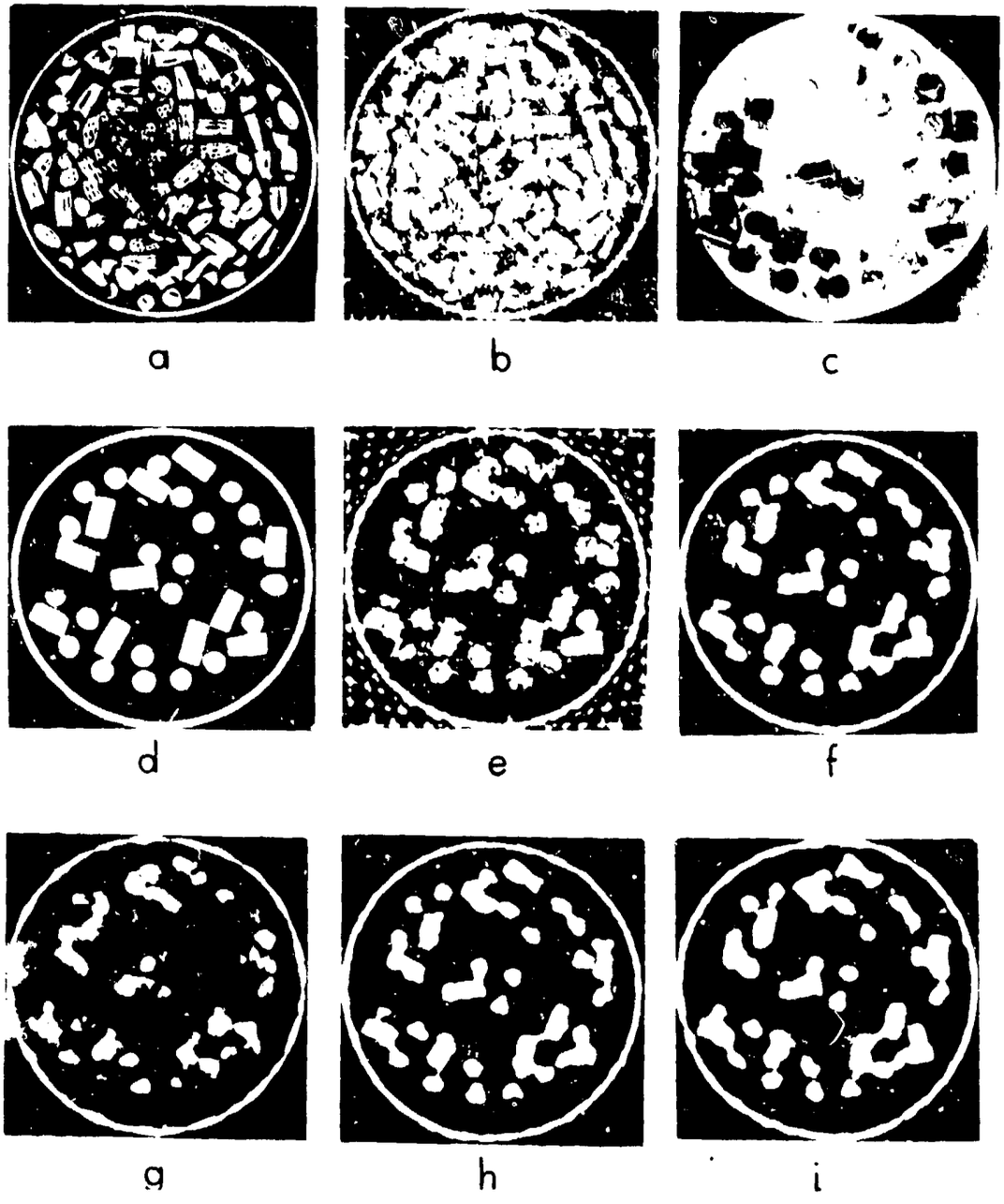

Figure 11. Reconstructions for Ballistic Mock-Ups

It may be noted here that both the monochromatic source and detector were collimated. Consequently, there was no scattered radiation from off-line elements of the test object that could reach the detector. This technique helped greatly in minimizing the problems associated with scattered radiation. Thus, these reconstructed images represent near optimum conditions with respect to interference from scattered radiation. In the short-time ballistic application it is not known how much scattered radiation will interfere with the reconstructed image. However, interior ballistic investigators have been routinely recording radiographs of interior ballistic processes for a number of years using polychromatic flash x-ray sources with no collimation at energies from 100 Kev up to 1 MeV. Propellant grains are clearly observed in these radiographs including perforations (~0.1 mm) and other small details. Clearly scattered radiation could not possibly be a serious problem or radiographs of this quality could not be produced. The interested reader is referred to References 9-12 and reports cited therein for examples of radiographs described above.

5. PROPOSED BRL SYSTEM

5.1 Geometrical Layout

It is clear from the work conducted at LANL, and described in Section 4, that a minimum of 15 to 20 views will be required in order to reconstruct a reasonable image, even for a low loading density configuration shown in Figure 11c. All of these projections should be acquired in a time frame that is short compared with any geometrical changes in the subject under investigation. For some ballistic systems, a time frame of 10 microseconds to 100 microseconds will be adequate. A chamber which simulates a large caliber configuration should have a diameter of between 150 and 200 mm. With these constraints in mind, two systems will be described which have the potential for satisfying these requirements. Details on x-ray sources and detectors will be given in a later section.

5.1.1 System 1. Investigators at two installations have constructed x-ray systems which have characteristics that meet some of these requirements. Trimble and Aseltine[20] at BRL have developed an x-ray cinematography system that has the capability of taking images at the rate of 100,000 pictures per second. Ritman, et al,[21] at the Mayo Clinic have designed a dynamic x-ray tomographic system called a Dynamic Spatial Reconstructor (DSR) which has a number of components similar to those used by Trimble and Aseltine. The DSR was designed to image the beating heart. It uses twenty-eight projections

---

[20] *J.J. Trimble and C.L. Aseltine, "Flash X-Ray Cineradiography at 100,000 FPS," The Seventh Symposium (International) on Detonation, US Naval Academy, Annapolis, MD, 11-19 June 1981.*

[21] *E.L. Ritman, J.H. Kinsey, R.A. Robb, L.D. Harris, and B.K. Gilbert, "Physics and Technical Considerations in the Design of the DSR - A High Resolution Volume Scanner," American Journal of Roentgenology, Vol. 134, pp. 369-374, 1980.*

which can be acquired in 10 ms. A ballistic tomographic setup based on References 20 and 21 is shown in Figure 12. This is an axial view of the chamber containing propellant grains. The 17 sources, x-ray conversion screen, and the image intensifier detectors are co-planar. The system works as follows. The x-ray sources numbered 1, 5, 9, 13, and 17 are flashed simultaneously, producing five nonoverlapping shadowgraphs, or projections indicated on the x-ray conversion screen. These are then recorded by the gated image intensifiers focused on a particular portion of the screen. A second series of sources, 2, 6, 10, and 14, can then be pulsed but only after a time long enough to allow recovery of the conversion screen. The image retained on the screen should be less than five percent of its original value[22] or succeeding images will have a residual signal and will distort the reconstruction process. Therein lies the chief difficulty associated with this setup: finding a screen with both high x-ray conversion efficiency and short decay time. There exists another problem. As discussed in Section 3.2.2, a significant amount of forward scattering takes place during transmission of the radiation through the sample. This scattered radiation degrades the quality of the shadowgraph. Ordinarily, grids (Potter-Bucky grids)[23] constructed of lead can be placed in front of a screen to reduce the amount of scattered radiation. However, to be most effective, these grids should be focused towards the x-ray source, as in Figure 2. It is not possible to focus the grid for a single detector screen back to multiple sources, as in Figure 12. For example, a grid placed at region 1 on the conversion screen cannot be focused back to all sources 1, 2, 3, and 4 even though all of these sources will project at least a portion of the radiograph on region 1 of the conversion screen. In summary, two problems are encountered in implementing this system; viz., the recovery time of the converter screen and inadequate collimation.

5.1.2 System 2. The problems associated with the previous setup can be avoided by the arrangement shown in Figure 13. All detectors and sources are located in a single plane, and each source has its own detector screen. Moreover, the shadowgraph of the object must fall within the 10^{o} angle as is shown in Figure 13. With this arrangement the images do not overlap and all 17 x-ray sources can be fired simultaneously (within 1-2 μs). As was mentioned in Section 5.1, the chamber diameter is assumed to be 200 mm. Since the x-ray intensity decreases as $1/r^2$ it is desirable to minimize the source-to-detector distance. Geometrical calculations show that with these constraints the minimum distance from the source-to-detector is 4.6 metres, with the object being midway between the two. For these conditions, the radiograph or projection would be relatively poor in quality because of the finite effective size of the x-ray source. A large object-to-detector distance does have one advantage; some of the forward scattered radiation which has a broad angular distribution will miss the detector and reduce the unwanted background fogging. To reduce the finite source size problem an arbitrary figure of 2.5 was chosen for the source-to-object/object-to-

---

[22] *F.L. Ritman, Private Communication.*

[23] *S.C. Bushong, Radiological Science for Technologists, C.V. Mosby Co., St. Louis, Toronto, London, 2nd Edition, p. 197, 1980.*

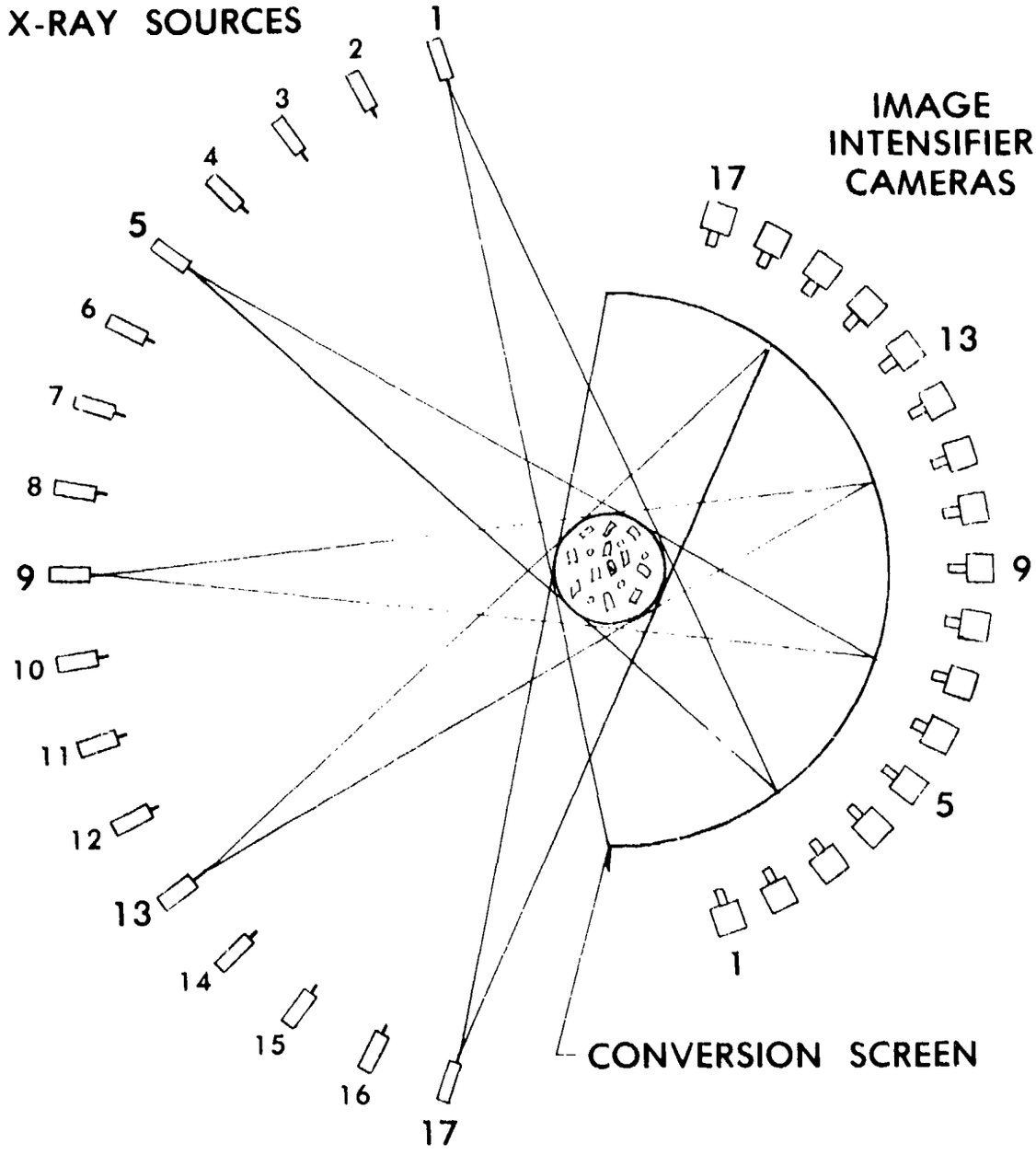

Figure 12. System 1 Configuration: Object Diameter, 180 mm

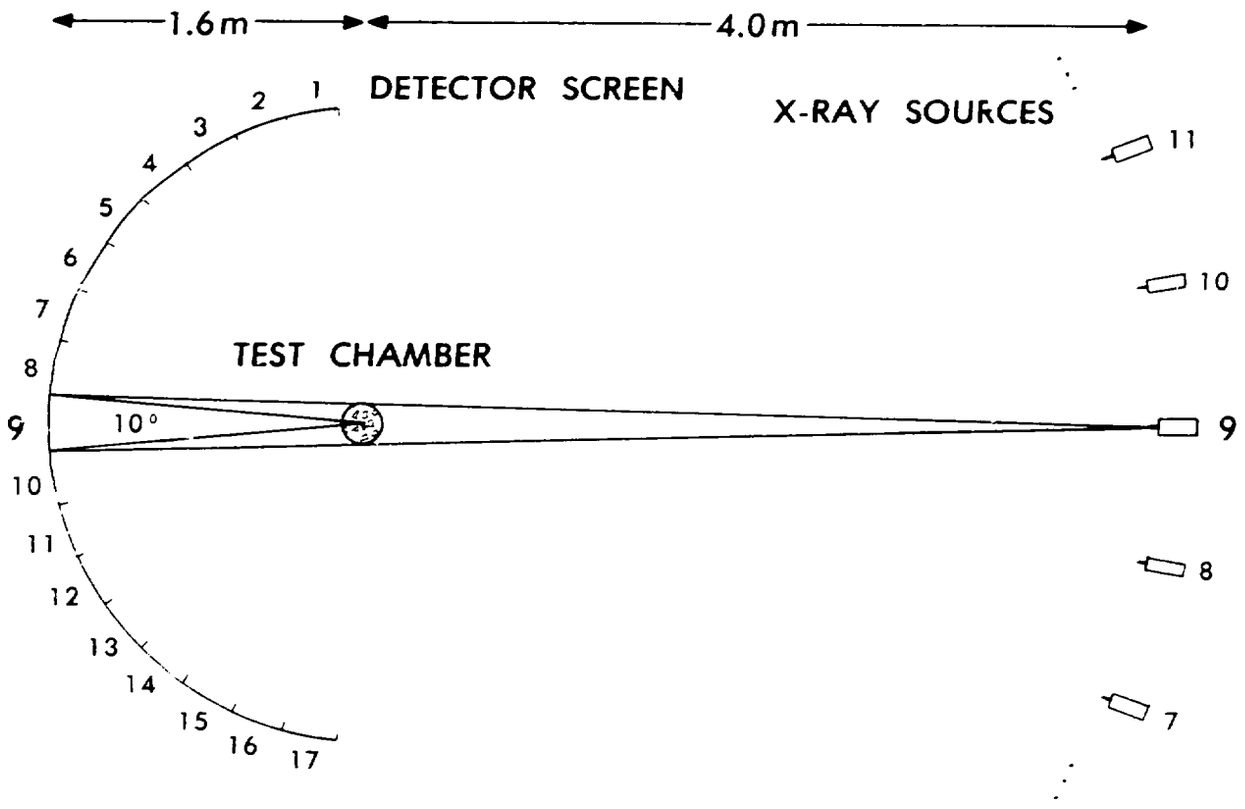

Figure 13. System 2 Configuration: Object Diameter, 200 mm

detector ratio. With these constraints the parameters shown in Figure 13 were determined. The source-to-detector distance was calculated to be 5.6 metres. This relatively large distance could lead to a problem with x-ray intensity at the detector. The setup described in Reference 12 employed similar dimensions. Nevertheless, useful radiographs were obtained

Individual detector arrays or screens for each source allows use of focused grids to reduce the amount of forward scattered radiation as is shown in Figure 2. In summary, System 2 has many advantages over System 1 but it must be demonstrated that there is sufficient x-ray intensity for an acceptable image.

5.2 X-Ray Sources

The choice of an x-ray source is driven largely by the time constraints imposed by the ballistic application, and the attenuation charactertistics of the chamber and propellant. As has been previously discussed, all projection data must be acquired within 50 to 100 microseconds. Medical x-ray units used in tomographic applications are largely of the thermionic type. The chief attraction of these tubes is their reliability, availability, and their small effective source size of 1 to 2 mm. However, there are certain drawbacks associated with these tubes; i.e., blooming or enlarging of the focus size as the x-ray output is increased, and a heel effect which results in a nonuniform intensity distribution across the sample being radiographed. The most important limitation, however, appears to be in the maximum pulse rate. The tubes used in the Mayo Clinic DSR[21] have a pulse width of 350 microseconds. This appears to be near the limit for thermionic tubes and is too slow for the intended ballistic application. Field emission tubes[24] have a number of advantages. Pulse-widths are on the order of 25 ns. A series of tubes can be pulsed at one-microsecond intervals. Hence, it is possible to take up to 20 shadowgraphs in 20 microseconds. Moreover, the design of a tube is such that there are no blooming or heel effects. Unfortunately, the effective source size is somewhat large (5 mm), and the shot-to-shot reproducibility required for tomographic application has not been tested. The problem of a large source size is purely geometrical in the sense that any finite size source will generate inferior shadowgraphs as the size increases. To alleviate this problem, the source-to-object over object-to-detector ratio can be increased. However, this leads to geometrical constraints on the system as is seen in Figure 13.

We recall here that in Section 4 tests were carried out using 200, 100, 50, and 25 points per projection. It was concluded that as few as 50 points could be used without seriously degrading the reconstruction (Figure 11i). These results will have an impact on the source-to-object-to-screen arrangement. Since only 50 points/projection are required for a good reconstruction, a relatively large source size can be used without degrading the reconstruction image. The field emission flash x-ray systems are commercially available and were used to obtain the radiographs in References 9 through 12.

---

[24] *F. Jamet and G. Thomer, Flash Radiography, Elsevier Scientific Publishing Company, Amsterdam, Oxford, New York, pp. 15-29, 1976.*

Although the output from these tubes contains characteristic radiation of the target material, these sources are essentially polychromatic having an output spectrum from 10 keV on up to the energy associated with the maximum operating voltage of the tube (100 keV - 1 MeV). This introduces another problem known as beam hardening. Because of two attenuation mechanisms (photoelectric effect and Compton effect) the softer x-rays are preferentially absorbed, leading to an alteration in the spectral distribution of the radiation emerging from the sample, with the average energy shifted to a higher value. This can be a particularly vexing problem in medical CT where one is trying to reconstruct images from a body that has materials containing calcium (bone) as well as hydrocarbons. The total attenuation cross section for calcium changes by 300 percent in going from 100 kev to 50 keV. However, the elements C, N, and O change between 20 percent and 30 percent over the same energy range. The large change due to calcium cross section can lead to artifacts in the reconstruction image. Considerable work has gone into addressing this problem and, for the application involving essentially a two-phase distribution of propellant and gas, this does not appear to be an important problem. The propellant-gas configuration is made up principally of H, C, N, and O with the mass fraction of H being small. The total attenuation cross sections of C, N, and O are virtually identical with each other at energies greater than 100 keV. With those materials at these energies we are dealing almost exclusively with the Compton effect where beam hardening problems are not of primary concern. Radioactive sources or accelerators could be used to generate a relatively monochromatic x-ray source which would avoid the beam hardening problem, but the former cannot easily be pulsed and the cost of assembling multiple accelerators would be prohibitive.

5.3 X-Ray Energies

As was mentioned in the last section, field emission tubes are available with x-rays that range in energy from 10 keV up to 1 MeV. What energy offers the best possibilities for the ballistic application? Absorption of low energy x-rays (below 60 keV) is caused by the photoelectric effect which produces little scattering and depends on Z^3, where Z is the atomic number of the absorbing material. In medical applications, this can be usefully exploited. The calcium-containing bone material has substantially greater absorption than the low atomic number tissue material. Consequently, superior, high-contrast radiographs are possible using low energy x-rays. The units for these x-rays are physically smaller and less expensive than the high energy units. Although the absorbed dose increases with the low energies, this is not a factor in the ballistic application. Because propellants are largely hydrocarbon materials, it may not be possible to take advantage of the greater contrast possibilities with low energy x-rays unless propellants are doped with contrast agents. Unfortunately, this would introduce unwanted chemical perturbations into the system. The attenuation of high energy x-rays (> 150 keV) is dominated by the Compton effect which generates undesirable forward scattered radiation. On the other hand, high energy tubes are more efficient at converting electron energy into x-rays and can generate larger doses, alleviating the detection problem. (The Hewlett-Packard 450-kV unit has more than ten times higher dosage compared with the 150-kV unit.) Additionally, the photoelectric effect is less significant at the higher energies and the beam hardening problem becomes less important. The LANL tests described in Section 4 indicated that acceptable data could be obtained

using a high energy source (316 keV, 468 keV). Radiation transport calculations in Section 2.2.2 also indicate the advantage of high energy. In summary, the above arguments suggest that the 450-kV field emission x-ray system or higher should be used in the initial testing.

6. DETECTION SYSTEMS

Each of the layouts previously described have shortcomings with respect to detector requirements. Consequently, two different detector configurations are being investigated. System 1 requires a detector with a fast recovery time so that image retention from overlapping projections will not be a problem. System 2 avoids this difficulty but, because of the large source-to-detector distances, needs a more sensitive detector. The reconstruction process is very sensitive to small variations in the recorded signal, so that strict requirements must be imposed on the detection system. Indeed, low noise, linearity, uniformity, and stability are needed to avoid the appearance of artifacts in the image. The dynamic range requirements will depend largely on the material under study. In medical tomography, 10^6 to 1 is desirable because of the large differences in x-ray absorption coefficients between different parts of the human body. In the ballistic application being considered in this study, the opposite problem exists. Because of the configuration of the propellant grains in the chamber, small changes in absorption coefficient are produced. Consequently, large dynamic ranges are not required but good contrast performance is necessary for low-noise data. The following paragraphs will discuss some of the potential solutions.

The two-dimensional detector intensifying screen used in References 20 and 21 was of the rare earth variety, gadolinium-oxy-sulfide doped with praseodymium ($Gd_2O_2S:Pr$). The measured lifetime for this screen was ten microseconds.[20] Although this proved to be sufficiently short for the 100,000 picture/second x-ray cinematographic system and the DSR, it has not yet been tested for the ballistic tomographic system. Figure 12 schematically shows a screen-detection setup. The x-rays interact with the conversion screen, producing visible light. The image is then collected by the appropriate optics and imaged on the image intensifier. A vidicon or solid state imaging device is then coupled to the output of the intensifier. The signal from this device is recorded on a video disc or magnetic tape system which is later transmitted to a computer for processing. The image intensifier, which can be of the magnetic focused type or the microchannel plate configuration, is used for several purposes. The large conversion screen format must be optically reduced to be compatible with the vidicon or solid state array detector. Optical losses are involved in this process and the large gain of the intensifier compensates for this. As is seen in Figure 12, 17 views are used for full reconstruction. Since the x-ray tubes are pulsed, the detectors must be gated so as to avoid a double exposure on the vidicon from succeeding pulses. The magnetically focused intensifiers are somewhat bulky and cumbersome to use. The microchannel plate intensifiers have limited diameter, uniformity problems, limited lifetime, and spatial resolution. However, the advantages of these devices are pulsing speed, low distortion, and variable

gain. This latter feature is important for insuring that all detector chains have the same sensitivity. Reference 25 should be consulted for more details on intensifiers.

For applications where a wide dynamic range is needed, charge coupled devices (CCD's) will be considered. These semiconductor devices, operating in the optical bandwidth of 120-1100 nm, are characterized y high quantum efficiency, approaching 70 percent in contrast to a photomultiplier tube of less than 20 percent efficiency, low noise level, and a dynamic range of around 5000 versus 100 for that of a photographic plate. They also offer excellent spatial resolution. The Texas Instruments CCD, for example, has an imaging area of 800 x 800 pixels, with each pixel measuring 15 μm on a side. With the amortization of the development costs of CCD's for the space telescope and TV cameras, the high cost of these devices should decline sufficiently and become a practical alternative for tomographic work.

If the Gd_2O_2S:Pr conversion screen decay time is too long for the ballistic application, a faster detector will be required. Organic scintillators used in nuclear spectroscopy have lifetimes of less than one microsecond. However, the sensitivity of these detectors is substantially lower than the rare earth materials. It may be possible to increase this sensitivity by arranging the scintillators in a configuration shown in Figure 2. Since only 15 - 20 views or projections will be used to reconstruct the image, it will not be necessary to have a high degree of resolution on each projection as was discussed in Section 4 and seen in Figures 11h and i. Consequently, the detectors can be arranged to integrate the signal over a relatively large area (Figure 2), increasing the signal at the output.

The sensitivity of the detector can be greatly increased by using inorganic scintillators such as NaI(Tl), $CdWO_4$, $ZnWO_4$, CsI(Tl), CsF, or $Bi_4Ge_3O_{12}$.[26,27] These detectors have selectively large x-ray absorption coefficients requiring from 3 to 10 mm thicknesses to absorb 90% of 150 keV x-rays. They can be grown as single crystals with good optical properties such that self-absorption of the visible emission radiation is not a problem. NaI(Tl) has an emission peak at 415 nm and is coupled to a photomultiplier tube with a S-20 photocathode which has a maximum sensitivity at 420 nm. This system was used in the early CT units. Although this material has the highest light output, it is hygroscopic and difficult to handle. In medical tomography, it is desirable to take 180 views in as short a time as possible

---

[25] *V. Chalmeton, "Microchannel X-ray Image Intensifiers," in Real-Time Radiologic Imaging: Medical and Industrial Applications, ASTM-STP-716, D.A. Garrett and D.A. Bracher, Eds., American Society for Testing and Materials, pp. 66-89, 1980.*

[26] *M.R. Farukhi, "Scintillation Detectors for CT Applications; An Overview of the History and State-of-the-Art," TP16REVA0679, Harshaw Chemical Company, Solon, OH, 1978.*

[27] *M.R. Farukhi, "Recent Developments in Scintillation Detectors for X-Ray CT and Positron CT Applications," TP211281, Harshaw Chemical Company, Solon, OH, 1981.*

to avoid blurring due to patient movement. Consequently, the decay time of these scintillators is of great importance since the signal from one view should decay to less than 5% of the original signal strength before another view can be acquired. Although the primary decay for NaI(Tl) is approximately 230 ns, 3-4% afterglow from secondary processes can remain for up to 150 ms. For this reason, several other inorganic scintillators have been developed and are listed above. The integrated light output of these other materials is lower than the NaI(Tl); however, they, in general, do not have the long secondary afterglow decay time that is present in NaI(Tl).

These scintillators are coupled to photodiode detectors and constitute one of the newer advances in CT detection systems. They have the advantage of solid state detectors that they can be made in any shape or size, so that dense packing is not a problem and they can be individually collimated. The detection process is started when the incoming x-ray is absorbed by the scintillator and converted to visible radiation which, in turn, is detected by a silicon PN junction photodiode. The generated current is then amplified. These materials scintillate in the 400 to 550 nm wavelength range which is slightly removed from the peak sensitivity of the photodiodes which occurs at 750 nm. Because of this, there is a loss of sensitivity of between a factor of two and three from the maximum obtainable.

Returning to the Gd_2O_2S:Pr intensifying screen, the importance of image retention or afterglow will depend largely on the requirements of System 1 versus System 2. A long decay time will not be a problem for System 2 and, in fact, may increase the overall sensitivity of the system. Conventional radiographic film can be used in place of the gated image camera or photodiode array for permanent recording of the data. Data from densitometer analysis of the film subsequent to the firing can be used as input to the image reconstruction algorithm. Collimator grids consisting of alternate strips of lead and aluminum can be used adjacent to the screen to remove scattered x-rays. Furthermore, a honeycomb grid could be used in which the scintillating material, either liquid or solid, would be placed in the opening cells of the grid which would optically isolate the light output of each cell with respect to every other cell. Moreover, if the web of the honeycomb were made of a leaded material or coated with a leaded paint, it would also act as an x-ray collimator. Several studies[28-30] have been conducted on the efficiency of intensifying screen-film combinations which include such materials as calcium tungstate, gadolinium-oxy-sulfide doped with terbium, barium halide, and lanthanum-oxy-bromide doped with terbium. The rare-earth doped compounds show a greater sensitivity, especially at energies greater than 60 keV due to

---

[28] *L.E. Bryant, J.P. Lucero, and R.P. Espejo, "X-Ray Film/Intensifying Screen Study for Flash Radiography," H-P 5952-6838, Hewlett-Packard, McMinnville, OR, 1980.*

[29] *G. Hagemann, D. Tollner, D. Saure, and J. Freyschmidt, "Neue Verstaerkerfolien in der Klinischen Radiologie," Fortschr. Roentgenstr., Vol. 124, pp. 483-489, 1976.*

[30] *C.E. Dick and J.W. Motz, "Image Information Transfer Properties of X-Ray Fluorescent Screens," Med. Phys., Vol. 8, pp. 337-346, 1981.*

absorption edges. However, they also exhibit a broader pulse height distribution which, potentially, can result in larger statistical noise on the detected signal. The major shortcoming of these materials is that they are polycrystalline, and hence there is a limit to the thickness of the screen that can be used. As the screen is made thicker, the emitted luminescence is scattered and absorbed within the material and never reaches the film or detector. A compromise must be found between x-ray absorption thickness and optical translucency. Reference 30 discusses the absorption characteristics of these materials at energies up to 68 keV.

Tests were carried out at LANL to determine the largest detector area that can be used, consistent with a satisfactory image. The results were discussed in Section 4 and are shown in Figures 11h and i. It is clear that between 50 and 100 points per projection will be required so as not to seriously degrade the quality of the reconstruction. Although System 2 does not have a problem with the decay time of the detector, the large source-to-detector distances require good sensitivity so as to avoid statistical fluctuations, or quantum mottle. An efficient x-ray conversion material can be employed without regard to decay time. As was discussed earlier, the maximum size of an individual detector element was determined by testing its effect on the quality of the reconstructed image. The simplest detector system that can be used with System 2 is a combination collimator, conversion screen and x-ray photographic film, the technique ordinarily used in conventional medical radiology. This offers advantages in simplicity of data acquisition during the ballistic event. However, the resulting shadowgraphs must then be digitized in an image analyzer. Dynamic range and calibration also present problems. This method is seldom employed in medical tomography because of the long turnaround time for image analysis and processing. This time constraint, however, is not important in the analysis of a ballistic event since infrequently would there be more than a few tests in the course of a day.

As was discussed in an earlier section, fluctuations in the intensity of the detected signal can have a deleterious effect on the quality of the reconstructed image. This can come about simply because, with so few x-ray photons, there is a statistical fluctuation in the numbe of photons at the detector. This fluctuation is proportional to $\sqrt{N}$, where N is the number of x-ray photons. The fewer the number of detected photons, the more severe the problem of noise becomes. For example, 25 photons will produce a variation of 20 percent in the detected signal. There is another source of quantum mottle. The absorption and optical conversion of a single x-ray photon does not necessarily produce exactly the same number of visible photons for each interaction. This phenomenon is referred to as "noise equivalent absorption" and further compounds the fluctuation problem. Thus, the fraction of x-ray photons absorbed does not completely determine how well the x-ray imaging detector is performing with respect to picture noise. Reference 31 gives more details on this problem.

---

[31] *J.D. Kingsley, "X-Ray Phosphors and Screens," in Real-Time Radiologic Imaging: Medical and Industrial Applications, ASTM-STP-716, D.A. Garrett and D.A. Bracher, Eds., American Society for Testing and Materials, pp. 98-112, 1980.*

As was pointed out in a recently granted US patent, Reference 32, newer liquid scintillation detectors can overcome many of the shortcomings of crystal detectors and may be the detector of choice for tomographic studies. In conventional liquid scintillation detectors, the x-ray photons interact with the material by undergoing Compton scattering, whereby the scattered photons are deflected into the collimator plates where they are absorbed, producing no optical output. Also, these detectors have low quantum detection efficiency, so that a detector cell length of 20 cm is not uncommon.

These problems have been overcome by the use of high Z value compounds in the scintillator liquid. Typically, fluoro compounds and bromonaphthalene have been used. The x-ray absorption of the solvent may be improved by adding organic solutes such as lead and tin alkyls. Such liquids offer quantum detection efficiences of 90% and an attenuation length of around 7 mm in the 70-150 keV x-ray energy region. Also, the fluorescence speed is in the nanosecond rather than the microsecond regime typical of crystal scintillation detectors. Added advantage is a smaller minimum cell size allowing better image resolution.

In summary, the search for a detector array will take two directions. An effort will be made to find one with the maximum sensitivity and minimum fluctuation. This can be used in the system shown in Figure 13. A second system should have a recovery time compatible with the recording requirements for the ballistic event (Figure 12).

7. CONCLUSIONS

Thus far, this study has established a number of critical requirements on a tomographic system for ballistic applications. First and foremost, it showed that with 15 to 20 views, under static conditions, good reconstruction of density profiles of a fluidized propellant grain, combustion gas system may be obtained. Second, conventional field emission x-ray sources can provide the time resolution required for ballistic application. Third, dynamic resolution, even when the atomic numbers of the materials studied only differ slightly, is not a problem with a state-of-the-art detector array. Fourth, as few as 50 points per projection will give a reasonable reconstruction. Fifth, a statistical reconstruction technique, such as MENT, is the best algorithm when the number of views is limited. Sixth, for studying low pressure events, such as ignition, thin-walled steel chambers can be used with high energy x-rays. Seventh, tomography can be obtained in the microsecond regime.

The remainder of this feasibility study will address the problem of the selection of the best detector array with the recovery time and sensitivity required for the reconstruction algorithm and run tests on the best arrangement of sources and detectors. The scattering problem from multiple sources will also be examined at this time.

---

[32] *D.A. Cusano and F.A. DiBianca, Scintillator Detector Array, US Patent 4262202, April 1981.*

Our recommendation is to build the initial system to generate tomograms of slices of the object to be studied. This will allow the use of currently available reconstruction algorithms. Concurrently with this task, the development of truly three-dimensional algorithms should be pursued. With the availability of such a code the system can be upgraded to its full three-dimensional capability. Ballistic tomography has the potential of considerably adding to our knowledge of diverse aspects of ballistics. We have already been able to demonstrate that under static conditions it can give information which was heretofore inaccessible by any experimental means.

ACKNOWLEDGMENT

It is a pleasure to acknowledge a number of useful discussions with our colleague, Dr. George Thomson, and Drs. E. Ritman and J. Kinsey of the Mayo Clinic. We thank Mr. Walter Van Antwerp for making the TIGER code available for our use.

REFERENCES

1. J. Radon, "Ueber die Bestimmung von Funktionen durch ihre Integralwerte laengs gewisser Manningfaltigkeiten," Berichte Saechsische Akad. Wiss., Vol. 69, pp. 262-277, 1917.

2. R.A. Brooks and G. DiChiro, "Principles of Computer Assisted Tomography (CAT) in Radiographic and Radioisotopic Imaging," Phys. Med. Biology, Vol. 21, No. 5, pp. 689-732, 1976.

3. G. Herman, Image Reconstruction from Projections, Academic Press, New York, 1980.

4. R. Gordon, "A Tutorial on ART," IEEE Transactions on Nuclear Science, NS-21, pp. 78-93, 1974.

5. G. Herman, "ART: Mathematics and Applications," J. Theor. Biology, Vol. 42, pp. 1-32, 1973.

6. L.A. Shepp and J.B. Kruskal, "Computerized Tomography: The New Medical X-Ray Technology," Amer. Mathematical Monthly, Vol. 85, pp. 420-439, 1977.

7. R.N. Bracewell and A.C Riddle, "Inversion of Fan Beam Scans in Radio Astronomy," Astrophys. J., Vol. 150, pp. 427-434, 1967.

8. G. Minerbo, "MENT: A Maximum Entropy Algorithm for Reconstructing a Source from Projection Data," Computer Graphics and Image Processing, Vol. 10, pp. 48-68, 1979.

9. U. Hornemann, "Investigation of Propellant Combustion in X-Ray Transparent Gun Tubes," Ernst-Mach-Institut/Abteilung fuer Ballistik Report No. 3/79, Weil am Rhein, West Germany, 1979.

10. T.C. Minor, "Characterization of Ignition Systems for Bagged Artillery Charges," ARBRL-TR-02377, USA ARRADCOM/Ballistic Research Laboratory, Aberdeen Proving Ground, MD, 1981 (AD A108119).

11. A.W. Horst and T.C. Minor, "Ignition Induced Flow Dynamics in Bagged Charge Artillery," ARBRL-TR-02257, USA ARRADCOM/Ballistic Research Laboratory, Aberdeen Proving Ground, MD, 1980 (AD A090681).

12. W.R. Burrell and J.L. East, "Effects of Production Packing Depth and Ignition Techniques on Propelling Charge Reaction and Projectile Response," NSWC/DC TR-3705, Naval Surface Weapons Center, Dahlgren, VA, 1979.

13. J.A. Halbleib and W.H. Vandevender, "TIGER: A One-Dimensional Multilayer Electron/Photon Monte Carlo Transport Code," SLA-73-1026, Sandia Laboratories, Albuquerque, NM, 1974.

14. A.L. Broz, "Methodology Investigation of Techniques for In-Bore Flash Radiography," TECOM Project No. 7-CO-PB5-AP1-086, Material Testing Directorate, Aberdeen Proving Ground, MD, 1977 (AD B0228342).

15. D.L. Snyder and J.R. Cox, "An Overview of Reconstructive Tomography and Limitations Imposed by a Finite Number of Projections," in Reconstruction Tomography in Diagnostic Radiology and Nuclear Medicine, M.M. Ter Pogossian, et al, editors, University Park Press, Baltimore, MD, 1977.

16. D.M. Joseph and R.A. Schulz, "View Sampling Requirements in Fan Beam Computed Tomography," Med. Phys, Vol. 7, No. 11, 1980.

17. K.T. Smith, D.C. Solman, and S.L. Wagner, "Practical and Mathematical Aspects of the Problem of Reconstructing Objects from Radiographs," Bulletin of the American Math. Society, Vol. 83, pp. 1227-1270, 1977.

18. R.A. Crowther, D.J. DeRosier, and A. Klug, "The Reconstruction of a Three-Dimensional Structure from Projections and Its Applications to Electron Microscopy," Proc. Royal Society London, Vol. A317, pp. 319-340, 1910.

19. R.P. Kruger, "Nonmedical Applications of Computed Tomography to Power Capacitor Quality Assessment," IEEE Transactions on Nuclear Science, NS-28, pp. 1721-1725, 1981.

20. J.J. Trimble and C.L. Aseltine, "Flash X-Ray Cineradiography at 100,000 FPS," The Seventh Symposium (International) on Detonation, US Naval Academy, Annapolis, MD, 11-19 June 1981.

21. E.L. Ritman, J.H. Kinsey, R.A. Robb, L.D. Harris, and B.K. Gilbert, "Physics and Technical Considerations in the Design of the DSR - A High Resolution Volume Scanner," American Journal of Roentgenology, Vol. 134, pp. 369-374, 1980.

22. E.L. Ritman, Private Communication.

23 [illegible]. Bushong, Radiological Science for Technologists, C.V. Mosby Co., St. Louis, Toronto, London, 2nd Edition, p. 197, 1980.

[illegible]. F. James and G. Thomer, Flash Radiography, Elsevier Scientific Publishing Company, Amsterdam, Oxford, New York, pp. 15-79, 1976.

25. V. Chalmeton, "Microchannel X-Ray Image Intensifiers," in Real-Time Radiologic Imaging: Medical and Industrial Applications, ASTM-STP-716, D.A. Garrett and D.A. Bracher, Eds., American Society for Testing and Materials, pp. 66-89, 1980.

26. M.R. Farukhi, "Scintillation Detectors for CT Applications; An Overview of the History and State-of-the-Art," TP16REVA0679, Harshaw Chemical Company, Solon, OH, 1978.

27. M.R. Farukhi, "Recent Developments in Scintillation Detectors for X-Ray CT and Positron CT Applications," TP211281, Harshaw Chemical Company, Solon, OH, 1981.

28. L.E. Bryant, [illegible] Lucero, and R.P. Espejo, "X-Ray Film/Intensifying Screen Study for Flash Radiography," H-P 5952-6838, Hewlett-Packard, McMinnville, OR, 1980.

29. G. Hagemann, D. Tollner, D. Saure, and J. Freyschmidt, "Neue Verstaerkerfolien in der Klinischen Radiologie," Fortschr. Roentgenstr., Vol. 124, pp. 483-489, 1976.

30. C.E. Dick and J.W. Motz, "Image Information Transfer Properties of X-Ray Fluorescent Screens," Med. Phys., Vol. 8, pp. 337-346, 1981.

31. J.D. Kingsley, "X-Ray Phosphors and Screens," in Real-Time Radiologic Imaging: Medical and Industrial Applications, ASTM-STP-716, D.A. Garrett and D.A. Bracher, Eds., American Society for Testing and Materials, pp. 98-112, 1980.

32. D.A. Cusano and F.A. DiBianca, Scintillator Detector Array, US Patent 4262202, April 1981.

LIST OF SYMBOLS

A	measurement set
B	reconstruction set
b_j	basis function
D	region, object diameter
d	resolution
f(x)	function
G	projection data
g	function
I	radiation intensity
J	index
j	index
K	index
k	index
L_i	line i
N	minimum number of views
$s(t, \theta_k)$	filtered function
s	path length
P	area
R	radius
t	distance
x	position
y	position
Z	atomic number
δ	delta function
ϵ	denotes member of a set
η	entropy

θ	angle
μ	absorption coefficient
ν_o	maximum resolvable spatial frequency
ψ	opening angle

DISTRIBUTION LIST

No. of Copies	Organization
12	Administrator Defense Technical Info Center ATTN: DTIC-DDA Cameron Station Alexandria, VA 22314
1	HQDA (DAMA-ARZ-DO) ATTN: D.F. Verderame Washington, DC 20301
1	Commander US Army Materiel Development and Readiness Command ATTN: DRCDMD-ST 5001 Eisenhower Avenue Alexandria, VA 22333
1	Commander US Army Armament Research and Development Command ATTN: DRDAR-TDC Dover, NJ 07801
2	Commander US Army Armament Research and Development Command ATTN: DRDAR-TSS Dover, NJ 07801
1	Commander US Army Armament Research and Development Command ATTN: DRDAR-QAF-I, H. Guttwein Dover, NJ 07801
1	Commander US Army Armament Material Readiness Command ATTN: DRSAR-LEP-L Rock Island, IL 61299
1	Director US Army ARRADCOM Benet Weapons Laboratory ATTN: DRDAR-LCB-TL Watervliet, NY 12189

No. of Copies	Organization
1	Commander US Army Aviation Research and Development Command ATTN: DRDAV-E 4300 Goodfellow Blvd. St. Louis, MO 63120
1	Director US Army Air Mobility Research and Development Laboratory Ames Research Center Moffett Field, CA 94035
1	Commander US Army Communications Rsch and Development Command ATTN: DRSEL-ATDD Fort Monmouth, NJ 07703
1	Commander US Army Electronics Research and Development Command Technical Support Activity ATTN: DELSD-L Fort Monmouth, NJ 07703
1	Commander US Army Missile Command ATTN: DRSMI-R Redstone Arsenal, AL 35898
1	Commander US Army Missile Command ATTN: DRSMI-YDL Redstone Arsenal, AL 35898
1	Commander US Army Missile Command ATTN: DRSMI-RKC, D. Ifshin Redstone Arsenal, AL 35898
1	Commander US Army Tank Automotive Command ATTN: DRSTA-TSL Warren, MI 48090

DISTRIBUTION LIST

No. of Copies	Organization
1	Director US Army TRADOC Systems Analysis Activity ATTN: ATAA-SL White Sands Missile Range NM 88002
2	Commandant US Army Infantry School ATTN: ATSH-CD-CSO-OR Fort Benning, GA 31905
1	Naval Surface Weapons Center ATTN: E. Criscuolo Silver Spring, MD 20910
1	AFWAL ATTN: L. Gulley Wright Patterson AFB, OH 45433
1	National Bureau of Standards ATTN: A. Carasso Administration A-302 Washington, DC 20234
2	National Bureau of Standards Thermal Processes Division ATTN: H.G. Semerjian S. Ray Washington, DC 20234
1	National Bureau of Standards ATTN: D. Polansky Washington, DC 20234
1	National Institute of Health ATTN: G. DiChiro Bethesda, MD 20014
1	National Institute of Health National Heart, Lung, and Blood Institute ATTN: A. Berson Federal Building, Rm 312 7550 Wisconsin Avenue Bethesda, MD 20205

No. of Copies	Organization
2	Director Los Alamos National Lab ATTN: K.M. Hanson C. Mader Los Alamos, NM 87545
2	US Army Research Office ATTN: J. Chandra R.J. Lontz P.O. Box 12211 Research Triangle Park NJ 27709
2	Mathematics Research Center ATTN: K.T. Smith J. Nohel 610 Walnut Street Madison, WI 53706
1	Advanced Research and Applications Corporation ATTN: A.G. Lason 8150 Leesburg Pike Vienna, VA 22190
1	American Science and Engineers, Inc. ATTN: R.C. Chase 33-37 Broadway Arlington, MA 02174
2	Bell Telephone Labs., Inc. ATTN: M. Sondhi F. Shepp Murray Hill, NJ 07971
1	BDM Corp. ATTN: T.P. Goddard P.O. Box 2019 2600 Garden Road Monterey, CA 93940
1	General Electric Computer Research Medical Diagnostics Systems Program ATTN: T. Kincaid Schenectady, NY 12345

DISTRIBUTION LIST

No. of Copies	Organization
1	The Harshaw Chemical Company Crystal and Electronic Products Department ATTN: M.R. Farukhi Solon, OH 44139
1	Hewlett-Packard Corp. ATTN: F. Charbonnier 500 Linke Street McMinnville, OR 97128
1	Industrial Quality, Inc. ATTN: H. Berger P.O. Box 2397 Gaithersburg, MD 20879
1	MCI Optonix, Inc. ATTN: G. Zweig Horsehill Road P.O. Box One Cedar Knolls, NJ 07927
1	Princeton Scientific Instruments, Inc. ATTN: J.L. Lowrance P.O. Box 252 Kingston, NJ 08528
1	Scientific Research Associates, Inc. ATTN: H. McDonald P.O. Box 498 Glastonbury, CT 06033
1	Thorn EMI Gencom, Inc. ATTN: L.M. Lieberman 80 Express Street Plainview, NY 11803
2	Mayo Clinic Biodynamics Research Unit ATTN: E.L. Ritman J.H. Kinsey 200 First Street, S.W. Rochester, MN 55901
1	University of California Donner Laboratory ATTN: T.F. Budinger Berkeley, CA 94720
1	George Washington University School of Engineering and Applied Science ATTN: R. Goulard Washington, DC 20052
1	Massachusetts Institute of Technology Laboratory for Information and Decision Systems ATTN: A.S. Willsky Cambridge, MA 02139
1	University of North Carolina Bio-Medical Engineering Department ATTN: F.A. DiBianca Chapel Hill, NC 27514
1	Hospital of the University of Pennsylvania Department of Radiology ATTN: G.T. Herman 3400 Spruce Street Philadelphia, PA 19104
1	University of Pittsburgh ATTN: D. Sashin Pittsburgh, PA 15261
1	Stanford University Department of Physics ATTN: A. Maconski Palo Alto, CA 94305
1	University of Utah Department of Mathematics ATTN: F. Stenger Salt Lake City, UT 84112
1	Dr. G. Morgan 1912 Sheffield Court Severn, MD 21144
1	Richard P. Kruger Los Alamos National Laboratory, WX-3 Fabrication & Assembly, MS C914 Los Alamos, NM 87545

DISTRIBUTION LIST

No. of Copies	Organization	No. of Copies	Organization

Aberdeen Proving Ground

Dir, USAMSAA
ATTN: DRXSY-D
DRXSY-MP, H. Cohen
Cdr, USATECOM
ATTN: DRSTE-TO-F
Dir, USACSL, Bldg. E3516, EA
ATTN: DRDAR-CLB-PA
DRDAR-CLN
DRDAR-CLJ-L

USER EVALUATION OF REPORT

Please take a few minutes to answer the questions below; tear out this sheet, fold as indicated, staple or tape closed, and place in the mail. Your comments will provide us with information for improving future reports.

1. BRL Report Number _____

2. Does this report satisfy a need? (Comment on purpose, related project, or other area of interest for which report will be used.)

_____

_____

_____

3. How, specifically, is the report being used? (Information source, design data or procedure, management procedure, source of ideas, etc.) _____

_____

_____

4. Has the information in this report led to any quantitative savings as far as man-hours/contract dollars saved, operating costs avoided, efficiencies achieved, etc.? If so, please elaborate.

_____

_____

5. General Comments (Indicate what you think should be changed to make this report and future reports of this type more responsive to your needs, more usable, improve readability, etc.) _____

_____

_____

_____

6. If you would like to be contacted by the personnel who prepared this report to raise specific questions or discuss the topic, please fill in the following information.

Name: _____

Telephone Number: _____

Organization Address: _____

_____

_____

FOLD HERE

Director
US Army Ballistic Research Laboratory
ATTN: DRDAR-BLA-S
Aberdeen Proving Ground, MD 21005

NO POSTAGE
NECESSARY
IF MAILED
IN THE
UNITED STATES

OFFICIAL BUSINESS
PENALTY FOR PRIVATE USE, $300

BUSINESS REPLY MAIL
FIRST CLASS PERMIT NO 12062 WASHINGTON, DC
POSTAGE WILL BE PAID BY DEPARTMENT OF THE ARMY

Director
US Army Ballistic Research Laboratory
ATTN: DRDAR-BLA-S
Aberdeen Proving Ground, MD 21005

FOLD HERE